

On the impact of non-factorisable corrections in VBF single and double Higgs production

Frédéric A. Dreyer, Alexander Karlberg, and Lorenzo Tancredi

Rudolf Peierls Centre for Theoretical Physics, University of Oxford, Clarendon Laboratory, Parks Road, Oxford OX1 3PU

December 22, 2024

Abstract. We study the non-factorisable QCD corrections, computed in the eikonal approximation, to Vector-Boson Fusion single and double Higgs production and show the combined factorisable and non-factorisable corrections for both processes at $\mathcal{O}(\alpha_s^2)$. We investigate the validity of the eikonal approximation with and without selection cuts, and carry out an in-depth study of the relative size of the non-factorisable next-to-next-to-leading order corrections compared to the factorisable ones. In the case of single Higgs production, after selection cuts are applied, the non-factorisable corrections are found to be mostly contained within the factorisable scale uncertainty bands. When no cuts are applied, instead, the non-factorisable corrections are slightly outside the scale uncertainty band. Interestingly, for double Higgs production, we find that both before and after applying cuts, non-factorisable corrections are enhanced compared to the single Higgs case. We trace this enhancement to the existence of delicate cancellations between the various leading-order Feynman diagrams, which are partly spoiled by radiative corrections. All contributions studied here have been implemented in `proVBFH` v1.2.0 and `proVBFHH` v1.1.0.

PACS. 12.38.-t Quantum chromodynamics – 12.38.Bx Perturbative calculations

1 Introduction

Following the discovery of the Higgs boson in 2012 [1, 2], it has become a primary focus of the experimental program of the Large Hadron Collider (LHC) to measure its properties and in particular its couplings to itself and to the other Standard Model particles [3]. One of the key channels for studying the Higgs boson is the Vector-Boson Fusion (VBF) production mode, where the Higgs boson is produced together with two (typically) hard and forward jets. This process has been the focus of several recent fixed order theoretical calculations [4–10].

A common point between all these calculations is that they are performed in the factorised approximation, which corresponds to the limit where partons from the two colliding protons are treated as coming from two identical copies of QCD that interact exclusively through the electroweak sector. When all emissions are integrated over, this approximation is referred to as the structure function approach [11]. Due to colour conservation, this approach is exact up to NLO, but starts to be violated from NNLO onwards, where colour-singlet two-gluon exchanges between the incoming partons are neglected. Since these non-factorisable contributions are colour suppressed compared to their factorisable counterparts, it has generally been assumed that they can also safely be neglected [5]. Recently it has been shown that the impact of the non-factorisable corrections at NNLO can be estimated in the so-called eikonal approximation [12]. Although this calcu-

lation confirms that their impact is moderate, it was found that these contributions also receive a π^2 -enhancement due to their connection to the Glauber scattering phase, which partially overcomes the effects of colour suppression.

Given these findings, the purpose of this paper is two-fold. Firstly, we investigate the validity of the approximation employed in Ref. [12] for single Higgs production outside of tight VBF cuts, in order to estimate the leading non-factorisable corrections on the inclusive VBF cross section. We then conduct an in-depth phenomenological study of the factorisable and non-factorisable corrections, and establish the relative impact of the latter for a range of selection cuts and observables. Secondly, we extend the calculation of Ref. [12] to study the impact of non-factorisable corrections to the production of a pair of Higgs bosons in VBF. In this case, contrary to single Higgs, it is well known that the rather small LO cross-section is the result of delicate cancellations of more than one order of magnitude between the different Feynman diagrams that contribute to the process, shown in figure 5. While QCD radiative corrections in the factorisable approximation affect equally all Born diagrams and are not expected to spoil this cancellation, the same cannot be expected a priori for the non-factorisable ones. Indeed, as we will demonstrate in this paper, a modest difference in the relative radiative corrections can potentially lead to an enhancement of the total NNLO corrections both inclusively and at the differential level. This, together with the Glauber π^2 -enhancement discussed above, can make the non-factorisable corrections

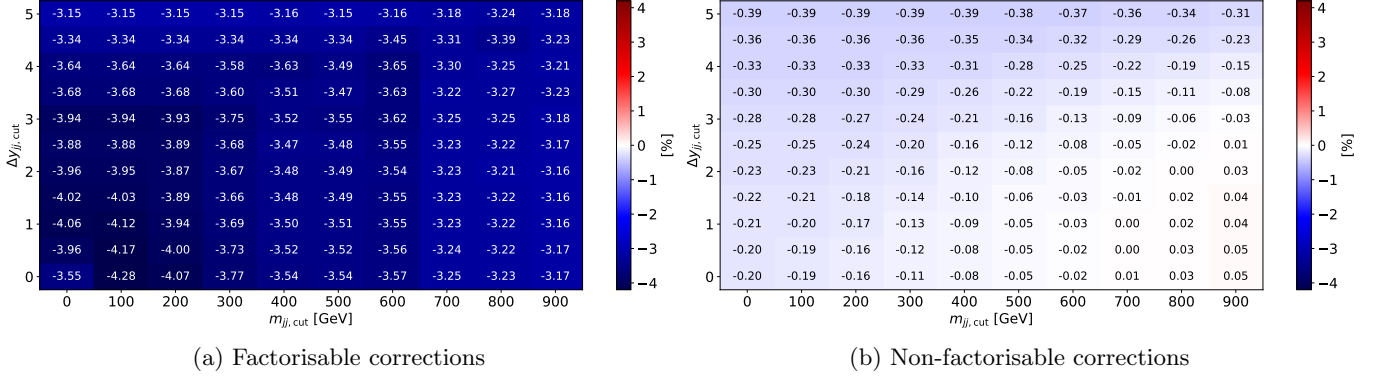


Fig. 1: Single Higgs VBF production: Ratio of the factorisable (a) and non-factorisable (b) NNLO corrections relative to LO for fiducial cross sections with two $R = 0.4$ anti- k_t jets satisfying $p_t > 25$ GeV and $|y_j| < 4.5$, as a function of the m_{jj} and Δy_{jj} selection cut.

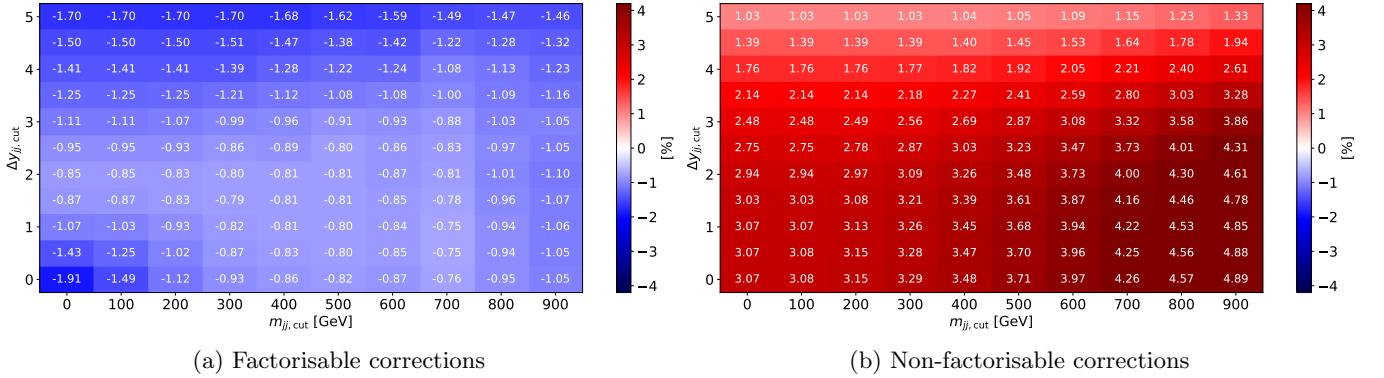


Fig. 2: Double Higgs VBF production: Ratio of the factorisable (a) and non-factorisable (b) NNLO corrections relative to LO for fiducial cross sections with two $R = 0.4$ anti- k_t jets satisfying $p_t > 25$ GeV and $|y_j| < 4.5$, as a function of the m_{jj} and Δy_{jj} selection cut.

of the same order or even dominant with respect to the factorisable ones.

In figure 1, we provide a summary of the impact of $\mathcal{O}(\alpha_s^2)$ corrections to single Higgs VBF production as a function of the selection cuts on the rapidity separation Δy_{jj} and the invariant mass m_{jj} . Figure 1a shows the ratio of the factorisable corrections to the LO cross section. The corrections have only a mild dependence on the cuts, decreasing from roughly -4% at low cuts to around -3% at larger cut values. The non-factorisable corrections shown in figure 1b on the other hand show a stronger dependence on the cuts. They increase in size with an increase in the Δy_{jj} cut, and decrease as the m_{jj} cut increases until they become positive but still small at very large m_{jj} cut values. In general they are suppressed by an order of magnitude compared to the factorisable corrections. In figure 2 we show the same comparison but for di-Higgs production. As can be seen in figure 2a the factorisable corrections have a more complicated dependence on the cut values compared to single Higgs VBF production, first decreasing with an increase in both cuts and then finally increasing in size as both cuts become large. The non-factorisable corrections

shown in figure 2b decrease with the Δy_{jj} cut and increase with the m_{jj} cut. In most of the plotted phase space they are larger in magnitude than their factorisable counterpart, and of opposite sign. In the phase space of experimental relevance where both cuts are large they are of the same size as the factorisable corrections.

We note that in addition to the non-factorisable corrections studied in this paper, a number of known perturbative corrections to VBF Higgs production are usually neglected. These include t/u -channel interference and s -channel contributions [13], single-quark line contributions [14], and loop induced interferences between VBF and gluon-fusion Higgs production [15]. These corrections are small within typical VBF cuts and we do not consider them here. The NLO corrections in the electroweak coupling have also been studied in Ref. [13].

The rest of the paper is structured as follows: in section 2 we provide a review of the known QCD corrections to VBF single Higgs production, and describe how to perform a similar estimate of the non-factorisable corrections to di-Higgs production in the eikonal approximation. In section 3 we compare factorisable and non-factorisable corrections

for VBF single Higgs production in a realistic setup. In section 4 we discuss the impact of the non-factorisable corrections to VBF di-Higgs production. In section 5 we give our conclusions.

2 QCD corrections in VBF Higgs production

2.1 Factorisable corrections

Both in single and double Higgs production via VBF, the Higgs bosons are emitted by the electroweak vector bosons exchanged between the two scattering partons. Schematically, the Born process for the emission of an arbitrary number of Higgs bosons can be depicted as in figure 3a.

In the factorised approximation, the VBF cross section is then expressed as a double deep inelastic scattering (DIS) process, see Fig. 3b, for which the cross section is given by [11]

$$d\sigma = \sum_V \frac{4\sqrt{2}G_F^3 m_V^8}{s} \Delta_V^2(Q_1^2) \Delta_V^2(Q_2^2) d\Omega_{\text{VBF}} \times \mathcal{W}_{\mu\nu}^V(x_1, Q_1^2) \mathcal{M}^{V,\mu\rho} \mathcal{M}^{V*,\nu\sigma} \mathcal{W}_{\rho\sigma}^V(x_2, Q_2^2). \quad (1)$$

Here $V = W^\pm, Z$ corresponds to the mediating boson with mass m_V and squared propagator Δ_V^2 , G_F is Fermi's constant, \sqrt{s} is the collider centre-of-mass energy, $Q_i^2 = -q_i^2$ and $x_i = Q_i^2/(2P_i \cdot q_i)$ are the usual DIS variables, $\mathcal{W}_{\mu\nu}^V$ is the hadronic tensor and $d\Omega_{\text{VBF}}$ is the VBF phase space. The matrix element of the vector-boson fusion sub-process is denoted as $\mathcal{M}^{V,\mu\nu}$.

The hadronic tensor can be expressed as

$$\mathcal{W}_{\mu\nu}^V(x_i, Q_i^2) = \left(-g_{\mu\nu} + \frac{q_{i,\mu} q_{i,\nu}}{q_i^2} \right) F_1^V(x_i, Q_i^2) + \frac{\hat{P}_{i,\mu} \hat{P}_{i,\nu}}{P_i \cdot q_i} F_2^V(x_i, Q_i^2) + i\epsilon_{\mu\nu\rho\sigma} \frac{P_i^\rho q_i^\sigma}{2P_i \cdot q_i} F_3^V(x_i, Q_i^2), \quad (2)$$

where we have defined $\hat{P}_{i,\mu} = P_{i,\mu} - \frac{P_i \cdot q_i}{q_i^2} q_{i,\mu}$ and $F_i^V(x, Q^2)$ are the standard DIS structure functions with $i = 1, 2, 3$.

For single Higgs production, given by the diagram T in Fig. 4, $\mathcal{M}^{V,\mu\nu}$ can be written as

$$\mathcal{M}^{V,\mu\nu} = g^{\mu\nu}. \quad (3)$$

By using the known DIS coefficient functions up to order α_s^3 [16–20], this can be used to evaluate the inclusive VBF cross section to single Higgs production up to N³LO in the factorised approximation. By combining an inclusive NNLO calculation with the corresponding fully differential NLO prediction for electroweak Higgs production in association with three jets [6], one can obtain fully differential results at NNLO through the projection-to-Born method [7] or the antenna subtraction method [8].

The factorisable QCD corrections to the di-Higgs process can be calculated in the same way as for its single Higgs analog, expressing the cross section in the form of

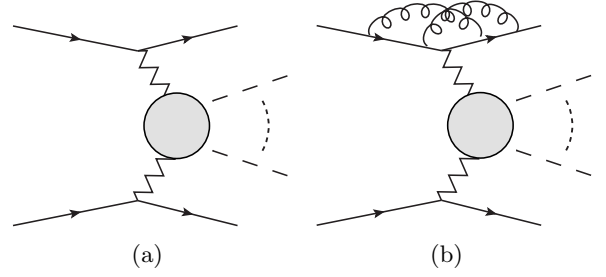


Fig. 3: Born diagram for the production of n Higgs bosons in VBF (a) and representative 2-loop factorisable corrections (b).

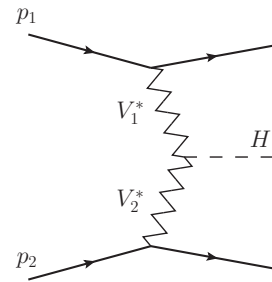


Fig. 4: Born diagram T for single Higgs VBF production.

eq. (1), but with \mathcal{M} now referring to the di-Higgs matrix element. The Higgs pair production process differs from the single Higgs case only at the interaction between the vector and Higgs bosons, where an additional Higgs can arise from an intermediate vector or Higgs boson, or from the $hhVV$ quartic coupling. The $VV \rightarrow hh$ sub-process at LO can be expressed as [21]

$$\mathcal{M}^{V,\mu\nu} = \left[\left(1 + \frac{4m_V^2}{\Delta_V} + \frac{6\nu\lambda}{\Delta_H} \right) g^{\mu\nu} + \frac{m_V^2}{\Delta_V} \frac{(2k_1^\mu + q_1^\mu)(k_2^\nu - k_1^\nu - q_1^\nu)}{m_V^2 - i\Gamma_V m_V} \right] + (k_1 \leftrightarrow k_2), \quad (4)$$

where we have defined the propagators

$$\Delta_V = (q_1 + k_1)^2 - m_V^2 + i\Gamma_V m_V, \quad \Delta_H = (k_1 + k_2)^2 - m_H^2 + i\Gamma_H m_H \quad (5)$$

and k_1, k_2 are the momenta of the final state Higgs bosons and λ and ν are the trilinear Higgs self-coupling and the vacuum expectation value of the Higgs field respectively. The matrix element arises from the four Feynman diagrams shown in Figure 5, which we label T_1, T_2, B_1 and B_2 . We stress here that, while we are including the bosons' widths for completeness, they play no role for the estimation of QCD corrections to Higgs production in VBF.

2.2 Non-factorisable corrections

The factorisable approach described above, which includes diagrams such as the one represented in figure 3b, is exact

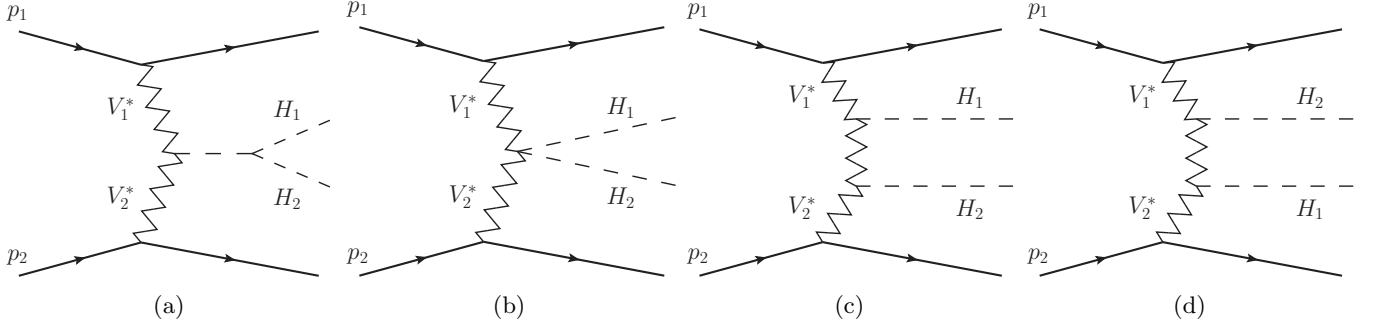


Fig. 5: Diagrams for Higgs pair production. (a) The T_1 topology. (b) The T_2 topology. (c) The B_1 topology. (d) The B_2 topology.

up to NLO due to colour conservation. At NNLO this is no longer true, as in particular two gluons in a colour singlet state can be emitted between the two quark lines, as shown in figure 6. As the gluons have to be in a colour singlet state, these diagrams will be colour suppressed compared to their factorisable counterparts. For this reason it has long been argued that they can be neglected when considering NNLO corrections to VBF [5].

Due to the complexity involved in computing the two-loop non-factorisable corrections, very little has been known about them beyond the fact that they are colour suppressed. However, very recently [12] significant progress was made, when it was shown that the corrections can be estimated within the eikonal approximation [22–25]. This calculation exploits the fact that when typical VBF cuts are applied, the VBF cross section can be expanded in the ratio of the leading jet transverse momentum over the total partonic centre-of-mass energy

$$\xi = \frac{p_{t,j_1}}{\sqrt{s}}. \quad (6)$$

In this kinematical configuration, the authors of Ref. [12] conclude that the non-factorisable corrections receive a π^2 -enhancement connected to the presence of a Glauber phase, which can partially compensate their colour suppression. Indeed, it turns out that for VBF single Higgs production, the non-factorisable corrections can contribute up to 1% in certain regions of phase space, making them larger than the factorisable N³LO corrections. In what follows we will use the same approximation to estimate the impact of non-factorisable corrections for the case of double Higgs production as well.

In order to see how the NNLO non-factorisable corrections can be estimated in the eikonal approximation both for single and double Higgs production, let us consider a generic VBF Born diagram, which we will call D , for the production of an in principle arbitrary number of Higgs bosons, see Fig. 3a. In what follows this diagram will represent either the Born diagram for VBF single Higgs production T of Fig. 4, or any of the Born diagrams for double Higgs production T_1 , T_2 , B_1 or B_2 in Fig. 5.

It is important to stress here that, somewhat counter-intuitively, we will be considering QCD corrections on

each single diagram separately, and not on the full Born matrix element. Since we are interested in computing the NNLO QCD corrections to this class of processes, we imagine dressing the diagram D with 1-loop or 2-loop QCD corrections, as depicted in Fig. 6, where we provide two representative diagrams for illustration only.

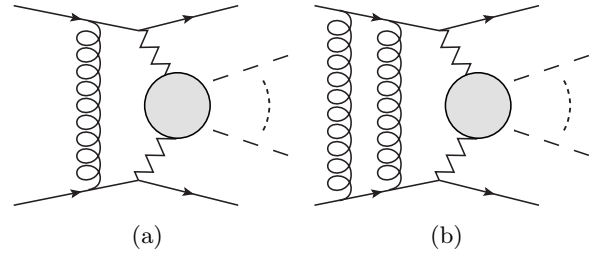


Fig. 6: Generic form of non-factorisable 1-loop (a) and 2-loop (b) corrections to the production of n Higgs boson.

It turns out that, at least up to two loops in QCD, we can limit ourselves to diagrams where the gluons are in a colour-singlet configuration, i.e. exchanged between the two quark lines. All other configurations do not contribute to the cross-section due to colour conservation. Therefore, the calculation of the one- and two-loop QCD corrections in the eikonal approximation reduces effectively to the corresponding calculation in QED, with the colour-averaged effective coupling

$$\tilde{\alpha}_s = \left(\frac{N_c^2 - 1}{4N_c^2} \right)^{1/2} \alpha_s. \quad (7)$$

Following Ref. [12], let us consider the process

$$q(p_1) + q(p_2) \rightarrow q(p_3) + q(p_4) + X(P) \quad (8)$$

where $X(P)$ can represent one or multiple Higgs bosons produced in vector-boson fusion. At leading order, we call the momenta flowing in the two vector bosons respectively

$$q_1 = p_1 - p_3, \quad q_2 = p_2 - p_4. \quad (9)$$

The leading term in the eikonal approximation can then easily be obtained by employing light-cone coordinates, which make transparent the separation between the dynamics in the plane spanned by the momenta of the incoming quarks and the plane transverse to them [22–25]. For a momentum k^μ we indicate by k^\pm the light-cone coordinates and by \vec{k} those in the transverse plane, i.e. we write

$$k^\mu = (k^+, k^-, \vec{k}), \quad k^\pm = \frac{k^0 \pm k^3}{\sqrt{2}}, \quad \vec{k} = (k_1, k_2), \quad (10)$$

and we choose a reference frame such that the incoming quark momenta have each one light-cone component different from zero

$$p_1^\mu = (0, p_1^-, \vec{0}), \quad p_2^\mu = (p_2^+, 0, \vec{0}).$$

It turns out that both at one and two loops, *at leading order in the eikonal approximation*, the quark propagators coupled to the soft gluons simplify and, after summing over all permutations of the gluons and the vector bosons, the quark propagators recombine in terms of delta functions of the light-cone components of the loop momenta. This allows one to decouple the light-cone dynamics from the one in the two-dimensional plane transverse to the momenta of the incoming quarks and one is left with the calculation of the effective *two-dimensional* loop diagrams shown schematically in Fig. 7.

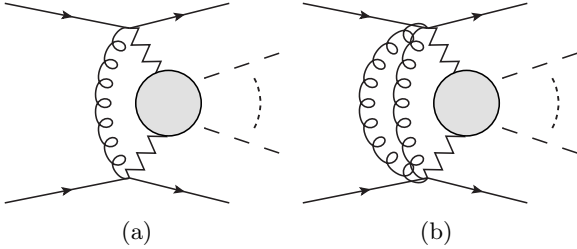


Fig. 7: Non-factorisable 1-loop (a) and 2-loop (b) corrections in the eikonal approximation. Notice that these are two-dimensional euclidean diagrams in the plane transverse to the incoming quark momenta.

With this, one can easily write the one- and two-loop QCD corrections in the eikonal approximation in a rather compact form. By calling \vec{q}_1 and \vec{q}_2 the transverse components of the momenta q_1 and q_2 in (9), and indicating schematically with $\{\vec{q}\}$ the set of transverse momenta of the Higgs bosons produced, we can write for the generic Born diagram D

$$\mathcal{M}_D^{(1)} = +i\tilde{\alpha}_s \chi_D^{(1)}(\vec{q}_1, \vec{q}_2, \{\vec{q}\}) \mathcal{M}_D^{(0)}, \quad (11)$$

$$\mathcal{M}_D^{(2)} = -\frac{\tilde{\alpha}_s^2}{2!} \chi_D^{(2)}(\vec{q}_1, \vec{q}_2, \{\vec{q}\}) \mathcal{M}_D^{(0)}, \quad (12)$$

where $\mathcal{M}_D^{(n)}$ are the corrections to the Born diagram D coming from the exchange of n gluons, $\chi_D^{(n)}(\vec{q}_1, \vec{q}_2, \{\vec{q}\})$ are

functions which depend on the (transverse) kinematics of the corresponding Born diagram and the effective coupling $\tilde{\alpha}_s$ was defined in eq. (7). Finally, the factor $1/2!$ comes from the symmetrisation of the two identical gluons [12]. We stress once more that, if we are interested in double Higgs production, this happens separately for each of the Born diagrams in Fig. 5. We also remind the reader that this is true as long as we limit ourselves to colour-singlet gluon exchange.

Given the considerations above, it is easy to see that QCD corrections to the Born diagram of single Higgs production T , or to $T_{1,2}$ for double Higgs, reduce to the computation of a two-dimensional one- or two-loop triangle-like integral, while the corrections to $B_{1,2}$, involve the computation of more complicated box-like loop integrals. Moreover, it should also be clear that for T , T_1 and T_2 , the QCD corrections only depend on the momenta \vec{q}_1 , \vec{q}_2 and are therefore equal in all three cases. Putting everything together, we find similarly to Ref. [12]

$$\chi_T^{(1)}(\vec{q}_1, \vec{q}_2) = \frac{1}{\pi} \int \frac{d^2 \vec{k}}{\vec{k}^2 + \lambda^2} \times \frac{\vec{q}_1^2 + M_V^2}{(\vec{k} - \vec{q}_1)^2 + M_V^2} \frac{\vec{q}_2^2 + M_V^2}{(\vec{k} + \vec{q}_2)^2 + M_V^2} \quad (13)$$

$$\chi_T^{(2)}(\vec{q}_1, \vec{q}_2) = \frac{1}{\pi^2} \int \left(\prod_{i=1}^2 \frac{d^2 \vec{k}_i}{\vec{k}_i^2 + \lambda^2} \right) \times \frac{\vec{q}_1^2 + M_V^2}{(\vec{k}_{12} - \vec{q}_1)^2 + M_V^2} \frac{\vec{q}_2^2 + M_V^2}{(\vec{k}_{12} + \vec{q}_2)^2 + M_V^2}, \quad (14)$$

where we defined $\vec{k}_{12} = \vec{k}_1 + \vec{k}_2$ and have introduced a fictitious gluon mass λ to regulate the residual IR divergences. Also, we have removed the dependence on the momenta $\{\vec{q}\}$ since for these diagrams $\vec{q}_1 + \vec{q}_2 = \vec{q}$.

Let us consider now the two box-like topologies, which have a non-trivial dependence on the momenta of the two Higgs bosons. Calling their momenta q_3 and q_4 and using $\vec{q}_4 = -\vec{q}_1 - \vec{q}_2 - \vec{q}_3$ (all momenta are incoming), we find

$$\chi_{B_1}^{(1)}(\vec{q}_1, \vec{q}_2, \vec{q}_3) = \frac{1}{\pi} \int \frac{d^2 \vec{k}}{\vec{k}^2 + \lambda^2} \times \frac{\vec{q}_1^2 + M_V^2}{(\vec{k} - \vec{q}_1)^2 + M_V^2} \frac{\vec{q}_2^2 + M_V^2}{(\vec{k} + \vec{q}_2)^2 + M_V^2} \frac{t + M_V^2}{(\vec{k} - \vec{q}_{13})^2 + M_V^2}$$

$$\chi_{B_1}^{(2)}(\vec{q}_1, \vec{q}_2, \vec{q}_3) = \frac{1}{\pi^2} \int \left(\prod_{i=1}^2 \frac{d^2 \vec{k}_i}{\vec{k}_i^2 + \lambda^2} \right) \times \frac{\vec{q}_1^2 + M_V^2}{(\vec{k}_{12} - \vec{q}_1)^2 + M_V^2} \frac{\vec{q}_2^2 + M_V^2}{(\vec{k}_{12} + \vec{q}_2)^2 + M_V^2} \frac{t + M_V^2}{(\vec{k}_{12} - \vec{q}_{13})^2 + M_V^2}$$

$$\chi_{B_2}^{(j)}(\vec{q}_1, \vec{q}_2, \vec{q}_4) = \chi_{B_1}^{(j)}(\vec{q}_1, \vec{q}_2, \vec{q}_3) \Big|_{\substack{\vec{q}_3 \leftrightarrow \vec{q}_4 \\ t \leftrightarrow u}}, \quad j = 1, 2. \quad (15)$$

where we put $\vec{q}_{ij} = \vec{q}_i + \vec{q}_j$ and defined in addition the “transverse-plane” Mandelstam variables $s = (\vec{q}_1 + \vec{q}_1)^2$,

$t = (\vec{q}_1 + \vec{q}_3)^2$, $u = (\vec{q}_1 + \vec{q}_4)^2$. Similarly to the previous case, we regulated the residual IR divergences with a gluon mass λ .

The integrals above can be computed in many different ways, most notably making use of the reduction of all 1-loop and certain 2-loop n -point functions, with $n \geq 3$, in $d = 2$ space-time dimension, to lower-point topologies. Also a direct computation of the integrals using their Feynman parameter representation can be attempted, which turns out to be particularly simple for the triangle integrals $\chi_T^{(1)}(\vec{q}_1, \vec{q}_2)$ and $\chi_T^{(2)}(\vec{q}_1, \vec{q}_2)$, see Ref. [12]. While the analytic computation is conceptually straightforward, the result, in particular for what concerns the box-type integrals, can become very cumbersome due to their dependence on a large number of scales and are not particularly illuminating.

Nevertheless, since we are dealing with two-dimensional euclidean integrals, it turns out to be entirely straightforward to produce very compact one-fold integral representations for them by extracting the logarithmic divergences as $\lambda \rightarrow 0$ and integrating directly on the 2-dimensional loop momenta in polar coordinates. This remains true at two loops, where one can first integrate out the gluonic one-loop sub-bubble, and then proceed in the very same way as for the one-loop integrals. This allows us to get all results as one-fold integrals over simple algebraic functions and at most powers of logarithms.

We write down the results for the one- and two-loop triangles as

$$\begin{aligned}\chi_T^{(1)}(\vec{q}_1, \vec{q}_2) &= -\ln\left(\frac{\lambda^2}{M_V^2}\right) + f_T^{(1)} \\ \chi_T^{(2)}(\vec{q}_1, \vec{q}_2) &= \ln^2\left(\frac{\lambda^2}{M_V^2}\right) - 2\ln\left(\frac{\lambda^2}{M_V^2}\right)f_T^{(1)} \\ &\quad + f_T^{(2)}\end{aligned}\quad (16)$$

and similarly for the boxes

$$\begin{aligned}\chi_{B_1}^{(1)}(\vec{q}_1, \vec{q}_2, \vec{q}_3) &= -\ln\left(\frac{\lambda^2}{M_V^2}\right) + f_B^{(1)} \\ \chi_{B_1}^{(2)}(\vec{q}_1, \vec{q}_2, \vec{q}_3) &= \ln^2\left(\frac{\lambda^2}{M_V^2}\right) - 2\ln\left(\frac{\lambda^2}{M_V^2}\right)f_B^{(1)} \\ &\quad + f_B^{(2)}\end{aligned}\quad (17)$$

where the function $f_T^{(j)}$ and $f_B^{(j)}$ depend on the corresponding transverse momenta and $\chi_{B_2}^{(j)}$ can be obtained from $\chi_{B_1}^{(j)}$ by swapping $\vec{q}_3 \leftrightarrow \vec{q}_4$ as in eq. (15). In order to write their analytic expression, we start off by parametrising the kinematics in the two-dimensional transverse plane as

$$\vec{q}_1 = (q_{1x}, 0), \quad \vec{q}_2 = (q_{2x}, q_{2y}), \quad \vec{q}_3 = (q_{3x}, q_{3y}) \quad (18)$$

with $q_4 = -q_1 - q_2 - q_3$, and we introduce the shorthand notation

$$\Delta_1 = (q_1^2 + M_V^2), \quad \Delta_2 = (q_2^2 + M_V^2), \quad \Delta_t = (t + M_V^2)$$

The functions can then be written as follows

$$f_T^{(1)} = -\int_0^{2\pi} \frac{d\xi}{\pi} \frac{\Delta_1 \Delta_2}{r_{13}} \left(\frac{\ln(\bar{r}_1)}{r_1 r_{12} r_{14}} + \frac{\ln(\bar{r}_3)}{r_3 r_{23} r_{34}} \right) + \left(\begin{matrix} r_1 \leftrightarrow r_2 \\ r_3 \leftrightarrow r_4 \end{matrix} \right) \quad (19)$$

$$f_T^{(2)} = -2 \int_0^{2\pi} \frac{d\xi}{\pi} \frac{\Delta_1 \Delta_2}{r_{13}} \left(\frac{\ln^2(\bar{r}_1)}{r_1 r_{12} r_{14}} + \frac{\ln^2(\bar{r}_3)}{r_3 r_{23} r_{34}} \right) + \left(\begin{matrix} r_1 \leftrightarrow r_2 \\ r_3 \leftrightarrow r_4 \end{matrix} \right) + \frac{4\pi^2}{3} \quad (20)$$

$$f_B^{(1)} = -\int_0^{2\pi} \frac{d\xi}{\pi} \frac{\Delta_1 \Delta_2 \Delta_t}{r_{13} r_{15} r_{35}} \left(\frac{r_{35} \ln(\bar{r}_1)}{r_1 r_{12} r_{14} r_{16}} + \frac{r_{15} \ln(\bar{r}_3)}{r_3 r_{23} r_{34} r_{36}} + \frac{r_{13} \ln(\bar{r}_5)}{r_5 r_{25} r_{45} r_{56}} \right) + \left(\begin{matrix} r_1 \leftrightarrow r_2 \\ r_3 \leftrightarrow r_4 \\ r_5 \leftrightarrow r_6 \end{matrix} \right) \quad (21)$$

$$f_B^{(2)} = -2 \int_0^{2\pi} \frac{d\xi}{\pi} \frac{\Delta_1 \Delta_2 \Delta_t}{r_{13} r_{15} r_{35}} \left(\frac{r_{35} \ln^2(\bar{r}_1)}{r_1 r_{12} r_{14} r_{16}} + \frac{r_{15} \ln^2(\bar{r}_3)}{r_3 r_{23} r_{34} r_{36}} + \frac{r_{13} \ln^2(\bar{r}_5)}{r_5 r_{25} r_{45} r_{56}} \right) + \left(\begin{matrix} r_1 \leftrightarrow r_2 \\ r_3 \leftrightarrow r_4 \\ r_5 \leftrightarrow r_6 \end{matrix} \right) + \frac{4\pi^2}{3} \quad (22)$$

with $r_{ij} = r_i - r_j$, $\bar{r}_j = -r_j/M_V^2$ and the six roots read where r_j^* indicates complex conjugation and

$$\begin{aligned}r_1 &= q_{1x} \cos \xi - \frac{iR_1}{\sqrt{2}}, \quad r_2 = r_1^*, \\ r_3 &= -(q_{2x} \cos \xi + q_{2y} \sin \xi) - \frac{iR_2}{\sqrt{2}}, \quad r_4 = r_3^*, \\ r_5 &= ((q_{1x} + q_{3x}) \cos \xi + q_{3y} \sin \xi) - \frac{iR_3}{\sqrt{2}}, \quad r_6 = r_5^*,\end{aligned}\quad (23)$$

$$\begin{aligned}R_1 &= \sqrt{2M_V^2 + q_1^2(1 - \cos 2\xi)} \\ R_2 &= \sqrt{2(M_V^2 + q_2^2) - 2(q_{2x} \cos \xi + q_{2y} \sin \xi)^2} \\ R_3 &= \sqrt{2(M_V^2 + t) - 2((q_{1x} + q_{3x}) \cos \xi + q_{3y} \sin \xi)^2}.\end{aligned}\quad (24)$$

The complex arguments and the three square-roots above might seem somewhat unappealing, in particular

because lengthy but fully analytic representation can be obtained for all these functions in terms of polylogarithms. In fact, if we limit ourselves to one-loop, the expressions are rather compact and we report them in appendix A. Nevertheless, our results involve only integrals of logarithms and exhibit a very high degree of symmetry, both moving from one to two loops and going from 3- to 4-point functions. Moreover it is straightforward to rewrite the integrals to make them explicitly real, at the price of introducing inverse trigonometric functions. Finally, as a curiosity, it turns out that performing the calculation in this way the results can be effortlessly generalised to higher-point integrals, i.e. for an arbitrary number of Higgs bosons in the final state.

With the definitions above, the non-factorisable QCD corrections to the total amplitude for single and double Higgs production can be written, respectively, as

$$\mathcal{M}_H = \sum_j \mathcal{M}_H^{(j)}, \quad \mathcal{M}_{HH} = \sum_j \mathcal{M}_{HH}^{(j)}, \quad (25)$$

where for single Higgs we have simply

$$\mathcal{M}_H^{(j)} = \mathcal{M}_T^{(j)}, \quad (26)$$

while for double Higgs we find

$$\mathcal{M}_{HH}^{(j)} = \mathcal{M}_{T_1}^{(j)} + \mathcal{M}_{T_2}^{(j)} + \mathcal{M}_{B_1}^{(j)} + \mathcal{M}_{B_2}^{(j)}, \quad (27)$$

which of course implies a much richer interference pattern. More explicitly, we find for the cross-section for single Higgs production

$$d\sigma_{H,\text{nf}}^{\text{NNLO}} = \tilde{\alpha}_s^2 \chi_{\text{nf}}^H(\vec{q}_1, \vec{q}_2) d\sigma^{\text{LO}} \quad (28)$$

where $d\sigma^{\text{LO}}$ is the leading-order cross section given in (1), $\tilde{\alpha}_s$ is the effective coupling in eq. (7), and the NNLO non-factorisable contributions only depend on the functions $f_T^{(j)}$ through

$$\begin{aligned} \chi_{\text{nf}}^H(\vec{q}_1, \vec{q}_2) &= \left[\chi_T^{(1)}(\vec{q}_1, \vec{q}_2) \right]^2 - \chi_T^{(2)}(\vec{q}_1, \vec{q}_2) \\ &= \left[f_T^{(1)} \right]^2 - f_T^{(2)}. \end{aligned} \quad (29)$$

As an illustration, and in order to compare this case to di-Higgs production, it is useful to compute the corrections in the limit where all transverse scales become small compared to the vector-boson mass, i.e. $\vec{q}_{1,2}^2 \ll M_V^2$. In that limit, all integrals become trivial and we find [12]

$$\chi_{\text{nf}}^H(\vec{q}_1, \vec{q}_2) = 1 - \frac{\pi^2}{3}. \quad (30)$$

In the case of double Higgs production, the form of the corrections is rather cumbersome but still entirely straightforward and we prefer to avoid writing down the

formulas explicitly. On the other hand, if we consider the same limit as above, i.e. $\vec{q}_{1,2}^2 \sim \vec{q}_{3,4}^2 \ll M_V^2$, formulas simplify considerably. In order to present the result, we divide the LO cross-section in three contributions as

$$d\sigma_{HH}^{\text{LO}} = d\sigma_{TT}^{\text{LO}} + d\sigma_{BB}^{\text{LO}} + d\sigma_{TB}^{\text{LO}}, \quad (31)$$

where $d\sigma_{TT}^{\text{LO}}$ is the contributions stemming solely from diagrams T_1 and T_2 , $d\sigma_{BB}^{\text{LO}}$ from B_1 and B_2 and $d\sigma_{TB}^{\text{LO}}$ from the interference of the two classes of diagrams, see Fig. 5. With this, we find that the non-factorisable corrections at NNLO take the suggestive form

$$\begin{aligned} d\sigma_{HH,\text{nf}}^{\text{NNLO}} &\sim \tilde{\alpha}_s^2 \left[\left(1 - \frac{\pi^2}{3} \right) (d\sigma_{TT}^{\text{LO}} + d\sigma_{TB}^{\text{LO}}) \right. \\ &\quad \left. + \left(\frac{5}{4} - \frac{\pi^2}{3} \right) d\sigma_{BB}^{\text{LO}} \right]. \end{aligned} \quad (32)$$

Eq. (32) shows that the three contributions to the Born cross-section for di-Higgs production can receive radiative corrections which are different at the 10% level. The cross-section for HH production at LO is the result of delicate cancellations of more than one order of magnitude between the three different contributions in eq. (31), as can be seen in table 1. These cancellations are a well known manifestation of the role that the Higgs boson has in restoring unitarity in the Standard Model. Since we are working in the eikonal approximation, one could therefore wonder whether this approximation could spoil these cancellations and induce in this way artificially large NNLO QCD corrections on the di-Higgs cross-section. As a matter of fact, eq. (32) suggests that QCD corrections do affect differently the various contributions to the di-Higgs cross-section enough to modify the cancellation pattern. Interestingly though, eq. (32) is valid in the limit of very small transverse momenta, where one expects the eikonal approximation to work well and the cross-section to be insensitive to any unitarisation issues. We are therefore lead to conclude that non-factorisable QCD corrections do have a potentially large impact on di-Higgs production and that this does not appear to be only a result of the approximation considered.

In figure 8, we show the $\tilde{\alpha}_s^2$ coefficient of each of the TT , TB and BB contributions as a function of a cut on the maximum transverse momentum, $\max(p_{t,j_1}, p_{t,H_1}) < p_{t,\text{max}}$. At small values of $p_{t,\text{max}}$ we can observe a convergence of these coefficients to the analytic expression given in eq. (32). Above $p_{t,\text{max}} \sim M_Z$ there is a transition to different numerical values of the coefficients, leading to an even larger spoliation of the cancellation present in the LO cross section. It is therefore clear that the conclusions drawn from eq. (32) remain true away from the small transverse momentum limit considered here.

Another interesting limit to study is the case where the Higgs bosons' transverse momenta are small, i.e. $\vec{q}_3^2, \vec{q}_4^2 \ll M_V^2$ which implies that $\vec{q}_1^2 \sim \vec{q}_2^2$. In this limit, it is easy to show that the cross section becomes

$$\begin{aligned}
d\sigma_{HH,nf}^{\text{NNLO}} \sim \tilde{\alpha}_s^2 \left\{ \left[\frac{1}{4} (x^4 + 8x^3 + 10x^2 - 12x + 5) + (x+1)(x+3) \log(x+1) - 2\text{Li}_2(-x) - \frac{\pi^2}{3} \right] d\sigma_{BB}^{\text{LO}} \right. \\
+ \left[\frac{1}{2} (x^3 + 3x^2 - 4x + 2) + \frac{1}{2} (x+1)(x+5) \log(x+1) - 2\text{Li}_2(-x) - \frac{\pi^2}{3} \right] d\sigma_{TB}^{\text{LO}} \\
+ \left. \left[(x-1)^2 + 2(x+1) \log(x+1) - 2\text{Li}_2(-x) - \frac{\pi^2}{3} \right] d\sigma_{TT}^{\text{LO}} \right\}. \quad (33)
\end{aligned}$$

where $x = \bar{q}_1^2/M_V^2 = \bar{q}_2^2/M_V^2$. First we notice that this result reproduces eq. (32) when $x \rightarrow 0$, as expected. As x grows the radiative corrections to the three contributions differ widely and in particular we see that as $x \rightarrow \infty$ the cross section takes the form

$$d\sigma_{HH,nf}^{\text{NNLO}} \sim \tilde{\alpha}_s^2 \left[x^2 d\sigma_{TT}^{\text{LO}} + \frac{1}{2} x^3 d\sigma_{TB}^{\text{LO}} + \frac{1}{4} x^4 d\sigma_{BB}^{\text{LO}} \right]. \quad (34)$$

In the limit where $\bar{q}_1^2 \sim \bar{q}_2^2 \sim M_V^2$, ie when $x = 1$ we obtain

$$\begin{aligned}
d\sigma_{HH,nf}^{\text{NNLO}} \sim \tilde{\alpha}_s^2 \left[\left(4 \log(2) - \frac{\pi^2}{6} \right) d\sigma_{TT}^{\text{LO}} \right. \\
+ \left(1 + 6 \log(2) - \frac{\pi^2}{6} \right) d\sigma_{TB}^{\text{LO}} \\
+ \left. \left(3 + 8 \log(2) - \frac{\pi^2}{6} \right) d\sigma_{BB}^{\text{LO}} \right], \quad (35)
\end{aligned}$$

which numerically reads

$$d\sigma_{HH,nf}^{\text{NNLO}} \sim \tilde{\alpha}_s^2 \left[1.13 d\sigma_{TT}^{\text{LO}} + 3.51 d\sigma_{TB}^{\text{LO}} + 6.90 d\sigma_{BB}^{\text{LO}} \right], \quad (36)$$

and leads us to conclude that the non-factorisable corrections can grow very rapidly with x , ie with the transverse momentum of the jets. We note that the eikonal approximation is strictly speaking only valid when $x \sim 0$ and that the rapid growth could be seen (at least in part) as a consequence of the breakdown of the approximation.

Before concluding this section, it is worth noting that at $\mathcal{O}(\alpha_s^2)$ there are both loop-induced and real emission diagrams that contribute to the non-factorisable corrections discussed above. Nevertheless, it is well known that real emission diagrams do not contribute to leading order in the eikonal approximation, and the whole cross-section in this limit stems from the virtual contributions only. This is also demonstrated by the fact that IR divergences cancel between the two-loop and the one-loop squared amplitudes. We stress here that the real emission diagrams have been computed for the single Higgs case in [26], and could be used to compute non-factorisable corrections beyond the leading eikonal approximation, once the full two-loop amplitudes become available.

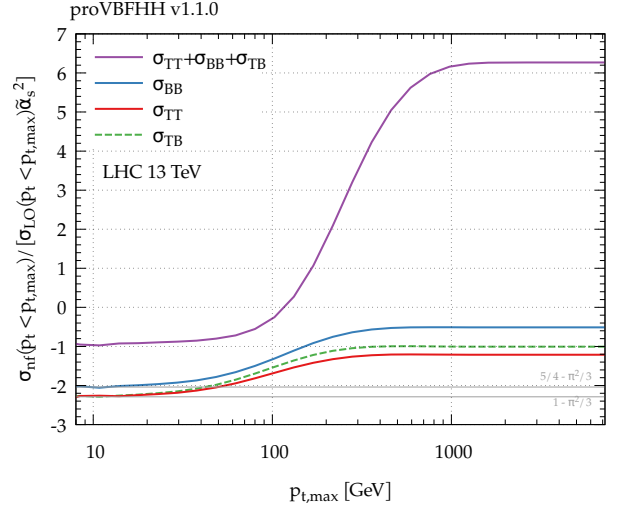


Fig. 8: $\tilde{\alpha}_s^2$ coefficient of the TT , TB and BB contributions to the NNLO non-factorisable corrections, normalised to the corresponding LO term, as a function of a cut on the maximum transverse momentum, $\max(p_{t,j_1}, p_{t,H_1}) < p_{t,\text{max}}$.

3 Results for single Higgs VBF production

3.1 Setup

In order to investigate the size of the various QCD corrections, we study 13 TeV proton-proton collisions, in a setup identical to Ref. [7]. We use a diagonal CKM matrix, full Breit-Wigners for the W , Z and the narrow-width approximation for the Higgs boson. We take the NNPDF 3.0 parton distribution functions at NNLO with $\alpha_s(M_Z) = 0.118$ (NNPDF30_nnlo_as_0118) [27], as implemented in LHAPDF-6.1.6 [28]. We consider five light flavours and ignore contributions with top quarks in the final state or internal lines. We set the Higgs mass to $M_H = 125$ GeV, compatible with the experimentally measured value [29]. Electroweak parameters are set according to known experimental values and tree-level electroweak relations. As inputs we use $M_W = 80.398$ GeV, $M_Z = 91.1876$ GeV and $G_F = 1.16637 \times 10^{-5}$ GeV $^{-2}$. For the widths of the vector bosons we use $\Gamma_W = 2.141$ GeV and $\Gamma_Z = 2.4952$ GeV. The central factorisation, μ_F , and

renormalisation, μ_R , scales are set to

$$\mu_0^2(p_{t,H}) = \frac{M_H}{2} \sqrt{\left(\frac{M_H}{2}\right)^2 + p_{t,H}^2}, \quad (37)$$

when computing factorisable corrections. We compute the residual scale uncertainties by varying this scale up and down by a factor 2 keeping $\mu_R = \mu_F$, which was shown in Ref. [7] to encompass almost the same scale uncertainty bands as a full 7-point scale variation (i.e. where μ_R and μ_F are varied independently by a factor 2 with $\frac{1}{2} \leq \frac{\mu_R}{\mu_F} \leq 2$). For the purpose of comparing these effects, we compute the non-factorisable corrections using the same central scale, which differs from the renormalisation scale choice $\mu_R = \sqrt{p_{t,j_1} p_{t,j_2}}$ in Ref. [12]. The residual scale uncertainties for these last predictions have been obtained using the full 7-point scale variation.

In the following we will discuss results both fully inclusively in the VBF jets, and under a set of representative VBF selection cuts. To pass our VBF selection cuts, events should have at least two jets with transverse momentum $p_t > 25$ GeV; the two hardest (i.e. highest p_t) jets should have absolute rapidity $|y| < 4.5$, be separated by a rapidity $\Delta y_{j_1,j_2} > 4.5$, have a dijet invariant mass $m_{j_1,j_2} > 600$ GeV and be in opposite hemispheres ($y_{j_1} y_{j_2} < 0$). We define jets using the anti- k_t algorithm [30], as implemented in `FastJet v3.1.2` [31], with radius parameter $R = 0.4$.

We compute all QCD corrections within the `proVBFH` framework [7, 9] which is based on results presented in Refs. [32–34, 6, 16–20]. As of version 1.2.0, the non-factorisable corrections of Ref. [12] have also been implemented in `proVBFH`. We evaluate the integrals of eqs. (19)–(22) using fourth order Runge-Kutta methods.

3.2 Validity of the eikonal approximation

The calculation of the non-factorisable NNLO corrections in VBF given in Ref. [12] is carried out as an expansion in ξ truncated to lowest order in ξ , see eq. (6). The authors argue that this ratio is typically of the order $\frac{1}{6}$, based on experimental measurements of the p_{t,j_1} and m_{jj} spectra [35, 36], and hence that the relative error associated with truncating the power expansion at the leading order is roughly $\frac{1}{36}$. This analysis is performed under the VBF cuts given in sec. 3.1 which guarantee large \sqrt{s} because of the requirement on the invariant mass of the di-jet system.

In this section we investigate in some detail how robust this approximation remains when no cuts are applied to the jets. Although such an inclusive setup is not of much phenomenological interest, it is of theoretical interest, given that not only the factorisable NNLO corrections are known fully inclusively, but also the N³LO ones [9].

In the left panel of figure 9 we show the normalised VBF cross section integrated in ξ , defined as

$$\Sigma(\xi) = \frac{1}{\sigma} \int_0^\xi \frac{d\sigma}{d\xi'} d\xi'. \quad (38)$$

We show the cross section fully inclusively and under VBF cuts. Under VBF cuts the cross section clearly lives below $\xi \sim 0.2$, whereas the fully inclusive cross section receives contributions all the way up to $\xi \sim 0.4$. However almost 85% of the events have $\xi < 0.2$ implying that the approximation used in Ref. [12] is valid in a large region of the inclusive VBF phase space. In fact, the average value of ξ is below 0.12 for all values of the rapidity of the Higgs Boson and for moderate transverse momenta, $p_{t,H}$, as can be seen in the two right panels of figure 9. At large $p_{t,H}$, the average value of ξ increases almost linearly with $p_{t,H}$ and hence the eikonal approximation starts to break down. This is not unexpected as $p_{t,H}$ is balanced by the jet transverse momenta, which by definition have to take moderate values in order to keep ξ small.

In the region of phase space where the eikonal approximation breaks down, i.e. when ξ becomes large, (28) is no longer valid. However, in this region the non-factorisable corrections are not expected to receive a Glauber phase enhancement partially mitigating the colour suppression, as this enhancement arises only in the eikonal limit.

3.3 Fiducial results

In this section, we provide results for both factorisable and non-factorisable corrections on differential and fiducial cross sections. Although they have been presented separately in Refs. [7, 12], we show here for the first time the combined factorisable and non-factorisable NNLO prediction to VBF Higgs production.

3.3.1 With VBF cuts

In figures 10 and 11 we compare the size of the factorisable and non-factorisable corrections to VBF Higgs production under the selection cuts of section 3.1. In the upper panels we show the NLO prediction. The lower panels show various predictions normalised to the NLO prediction. In blue we show the factorisable NNLO prediction with its associated scale uncertainty band. The red curve shows the combined NNLO factorisable and non-factorisable prediction. In the bulk of the phase space, the non-factorisable corrections are small and within the scale uncertainty bands. However, it is interesting to observe that for large p_{t,j_2} and $p_{t,H}$ the corrections can in certain regions become larger than the factorisable scale uncertainty. This makes the non-factorisable corrections of potential relevance in boosted Higgs boson searches. On the other hand it is clear from figure 9 that the eikonal approximation is not reliable at very high values of $p_{t,H}$, and the corrections should therefore be applied with care. A summary of the impact of $\mathcal{O}(\alpha_s^2)$ corrections on the fiducial cross section is shown in figure 1a as a function of the Δy_{jj} and m_{jj} selection cuts, requiring also two $R = 0.4$ anti- k_t jets with $p_t > 25$ GeV and $|y_j| < 4.5$. The corrections have only a mild dependence on the cuts, decreasing from roughly -4% at low cuts to around -3% at larger cut values. The non-factorisable corrections shown in figure 1b on the other hand show

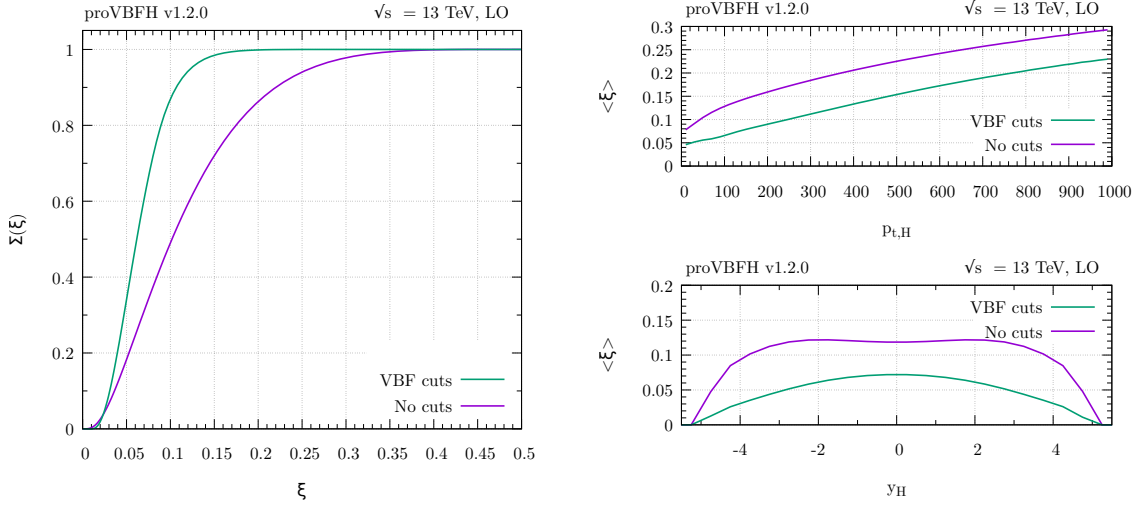


Fig. 9: (left): The normalised integrated cross section as a function of ξ fully inclusively (purple) and under the VBF cuts of sec. 3.1 (green) for single Higgs production through VBF. (right): The average of ξ as a function of y_H and $p_{t,H}$.

a stronger dependence on the cuts. In general they are suppressed by an order of magnitude compared to the factorisable corrections. They increase in size with an increase in the Δy_{jj} cut, and decrease as the m_{jj} cut increases. The first effect is related to the Glauber enhancement which grows with the separation of the jets. The decrease of the non-factorisable corrections as the m_{jj} cut increases is consistent with figure 11, where we observe that these corrections change sign around 2.5 TeV. It is important to keep in mind that these results will strongly depend on the choice of jet radius. Beyond LO the VBF cross section is well-known to be affected by real radiation escaping the tagging jets [37], while the NNLO non-factorisable corrections are independent of the jet radius. Therefore, one should compare the non-factorisable contribution not only to their factorisable counter-part, but also to the size of the scale uncertainty bands, particularly for large R values when the NNLO factorisable corrections become numerically small but their scale uncertainty remains large.

3.3.2 Without selection cuts

As discussed in section 3.2 the eikonal approximation is only formally valid when considering fiducial VBF production. It can however still provide a useful estimate of the size of the non-factorisable corrections in inclusive production. This is of particular interest, as the inclusive factorisable N³LO corrections are available for comparison in this regime.

In figure 12 we show in the lower panels for $p_{t,H}$ and $|y_H|$ in blue the factorisable NNLO prediction, and in green the factorisable N³LO prediction, both normalised to the NLO curve shown in the upper panel. We also show the combined factorisable and non-factorisable NNLO prediction in two setups: the non-factorisable corrections computed according to eq. (28) everywhere in phase space

(red) and the non-factorisable corrections computed according to eq. (28) when $\xi < 0.2$ and set to 0 otherwise (dashed-orange). This last procedure is used to verify that differential observables do not receive significant contributions from the large ξ region. We observe that in the bulk of the phase space the numerical difference between the red and the dashed-orange curves is very small - of the order of a few percent. It is therefore clear that the bulk of the non-factorisable corrections in the eikonal approximation come from the $\xi < 0.2$ region, even without VBF cuts. This is consistent with figure 9 which shows that the mean value of ξ is typically below 0.2. We observe that the non-factorisable NNLO corrections are typically larger than the factorisable N³LO ones, and that they are not covered by the NNLO scale variation uncertainties. In fact, the non-factorisable NNLO corrections are almost $\mathcal{O}(40\%)$ of the factorisable ones at this order. However we stress again that the non-factorisable corrections computed in the eikonal approximation do not necessarily provide reliable predictions in the full VBF phase space, as sub-leading terms can become relevant. It should also be noted that this large effect stems not from an enhancement of the non-factorisable effects, but rather from an order of magnitude decrease in the factorisable corrections when no cuts are applied.

4 Results for di-Higgs VBF production

We will now investigate the impact of non-factorisable contributions to the VBF Higgs pair production process. The electroweak parameters are set identically to the previous single Higgs study detailed in 3.1, with a width $\Gamma_H = 4.030$ MeV for the internal Higgs propagator, while the final state Higgs bosons remain in the narrow-width approximation. For the factorisable corrections the central

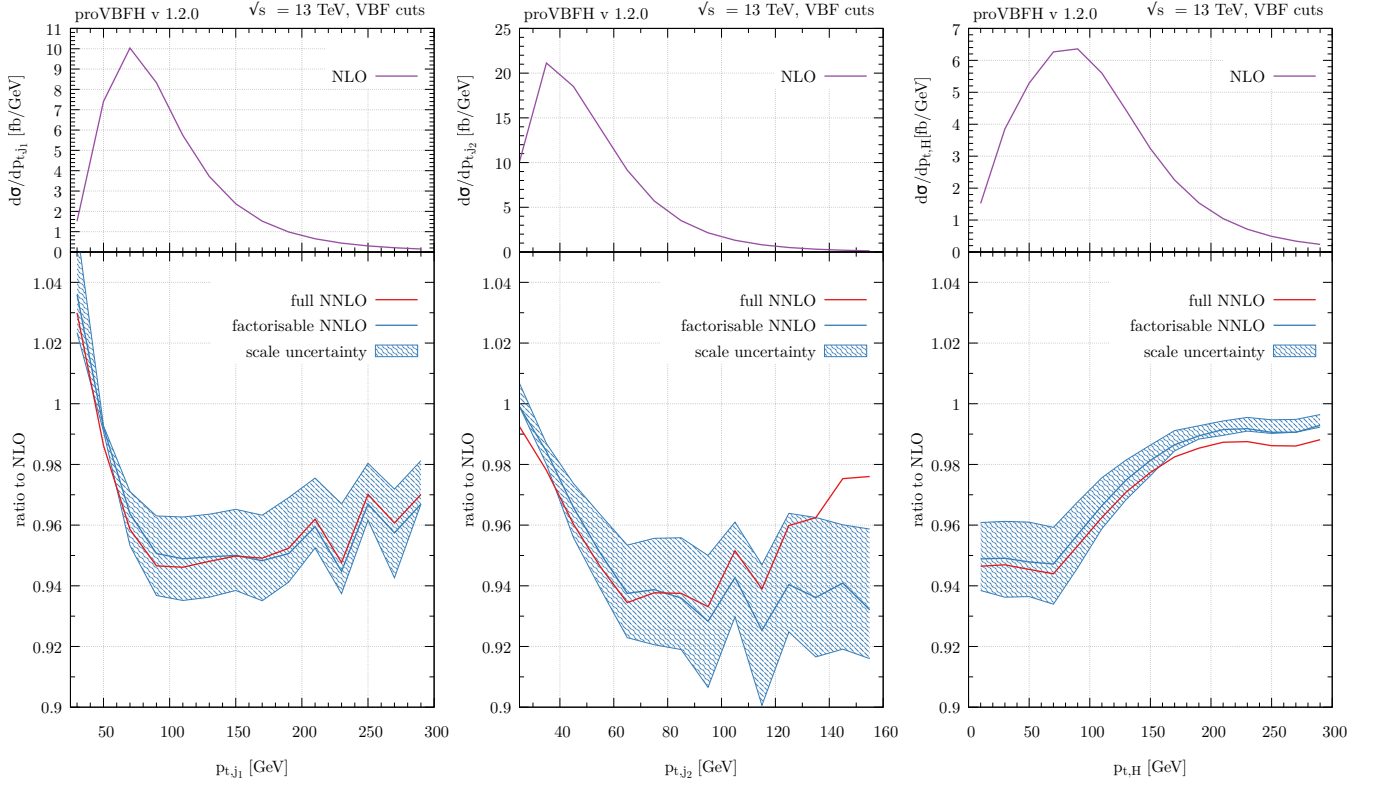


Fig. 10: Upper panel: NLO prediction for VBF production with cuts for the transverse momentum of the two leading jets and the Higgs boson. Lower panel: Ratio of the factorisable NNLO prediction to NLO (blue) and of the full NNLO prediction to NLO (red). The blue bands represent the scale uncertainty of the NNLO factorisable prediction.

renormalisation and factorisation scales are now set to

$$\mu_0^2(p_{t,HH}) = \frac{m_H}{2} \sqrt{\left(\frac{m_H}{2}\right)^2 + p_{t,HH}^2}, \quad (39)$$

and uncertainties from missing higher orders are again estimated by varying the scales symmetrically up and down by a factor two, as was discussed in section 3.1. For the non-factorisable corrections we pick the same central scales, but when showing the residual scale uncertainty envelope, we perform the full 7-point scale variation, i.e. varying independently μ_R and μ_F by a factor 2 but keeping the ratio to the interval $\frac{1}{2} \leq \frac{\mu_R}{\mu_F} \leq 2$. The NNLO corrections are calculated with `proVBFHH v1.1.0` [38, 39].

4.1 Validity of the eikonal approximation

Similarly to what we did for single Higgs production, we start by examining the validity of the eikonal approximation. We expect the eikonal approximation to be valid when all transverse scales are small compared to the total centre-of-mass energy. To test this statement quantitatively, we define

$$\xi_{HH} = \frac{\max\{p_{t,j1}, t, u\}}{\sqrt{s}}. \quad (40)$$

where t and u are defined as below eq. (15). In figure 13, we show in the left panel the normalised di-Higgs VBF cross section integrated in ξ_{HH} , both fully inclusively and under VBF cuts. Here we see that compared to the single Higgs process, the ξ_{HH} distribution with no cuts is contained to lower values below $\xi_{HH} \sim 0.25$. With VBF cuts the two distributions are very similar, and we therefore expect the eikonal approximation to be valid also in the di-Higgs process. In particular, from the right panel of figure 13, it is clear that the approximation only starts to break for very large transverse momentum values of the Higgs pair.

4.2 Fiducial results

In this section we discuss the impact of the non-factorisable NNLO corrections to di-Higgs VBF production computed in section 2.2. As was discussed there, the non-factorisable corrections are characterised by an interesting interference pattern which is not present in the single Higgs process. In table 1 we exemplify this by showing the LO fiducial cross section under the cuts of section 3.1 and their NNLO non-factorisable corrections. We split the cross section into the contribution coming from only the T_1 and T_2 topologies, σ_{TT} , only the B_1 and B_2 topologies, σ_{BB} and their interference, σ_{TB} , c.f. figure 5. As one can see, the di-Higgs cross section at LO is the result of cancellations

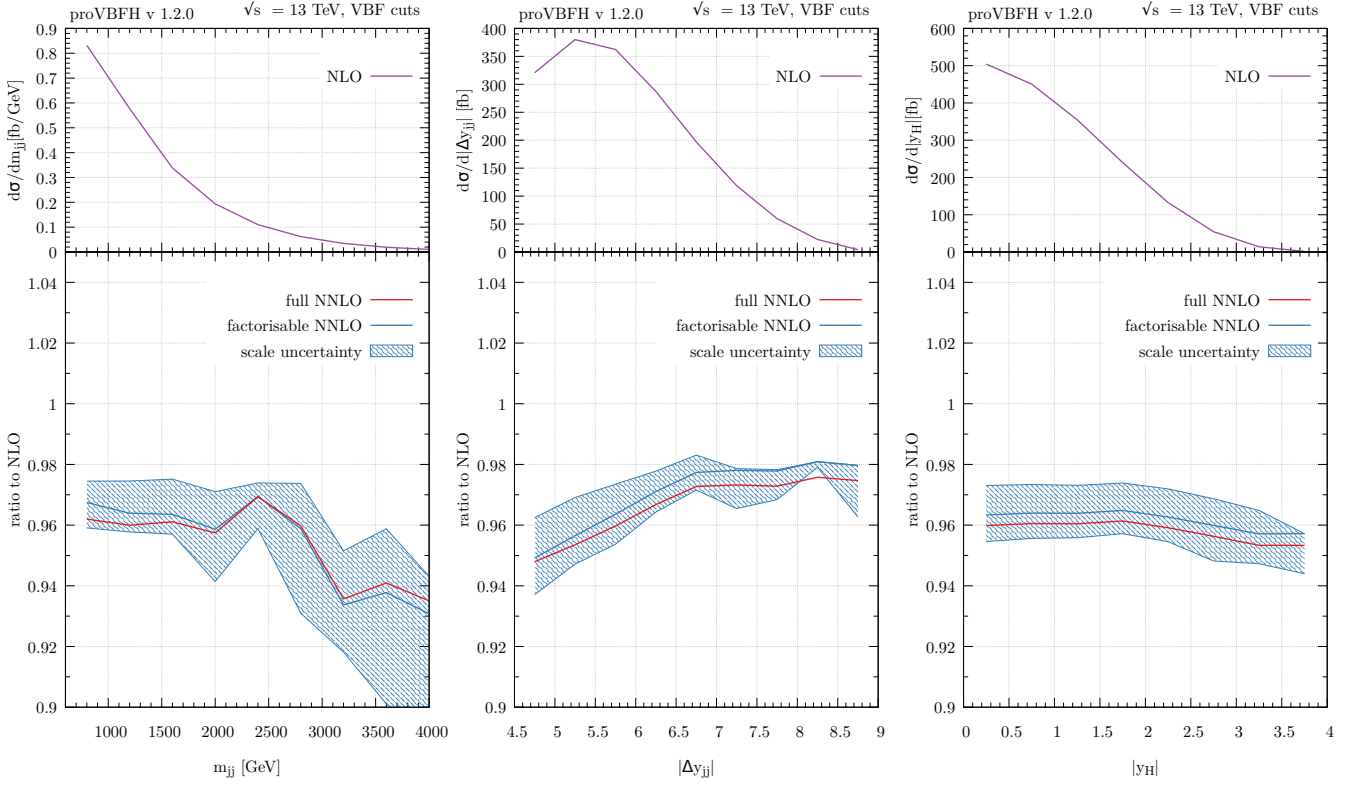


Fig. 11: Upper panel: NLO prediction for VBF production with cuts for the invariant mass and rapidity separation of the tagging jets, as well as for the rapidity of the Higgs boson. Lower panel: Ratio of the factorisable NNLO prediction to NLO (blue) and of the full NNLO prediction to NLO (red). The blue bands represent the scale uncertainty of the NNLO factorisable prediction.

$\lambda = M_V$	σ_{TT}	σ_{BB}	σ_{TB}	Σ
Born	10.393 fb	14.172 fb	-23.904 fb	0.662 fb
1-loop NF	0.339%	0.518%	0.399%	2.03%
2-loop NF	-0.667%	-0.658%	-0.666%	-0.50%
Full NF	-0.327%	-0.139%	-0.267%	1.52%

Table 1: Fiducial cross section for vector-boson fusion di-Higgs production at 13 TeV under the cuts of sec. 3.1. The first row indicates the Born contribution in femtobarn of the triangle diagrams, box diagrams and their interference. The second row shows the 1-loop squared non-factorisable (1-loop NF) correction in percent of the Born results for the same three contributions. The third row shows the same but for the 2-loop times tree-level non-factorisable (2-loop NF) contribution. The last row shows the same breakdown but for the sum of both contributions. The last column shows the sum of the contributions across each row.

spanning several orders of magnitude. For the individual sets of diagrams, the non-factorisable corrections are below 1% and one can show that the combined 1- and 2-loop contribution in each case is always negative. However, the total correction turns out to be positive and above 1%,

since the negative non-factorisable corrections on top of the already negative LO interference dominate slightly over the other two contributions. Indeed, since QCD corrections affects the four Born diagrams differently, the delicate cancellations which characterise the LO cross-section get spoiled and the total correction ends up being more than four times larger in magnitude than any of the individual ones. It is interesting to note that the relative correction to σ_{TT} of -0.327% is very close to the correction found in the single Higgs process of -0.32% under identical cuts (cf figure 1b), and hence that the enhancement in the total correction is not a consequence of the different kinematics of the di-Higgs system itself.

At the level of distributions this effect can become even more sizeable. To put the size of the NNLO non-factorisable corrections into context, we compare them to the factorisable NNLO corrections. In figure 14 we show the corrections to the two hardest jets, normalised to the NLO cross section. For low to moderate jet transverse momenta the non-factorisable corrections are at the few percent level and typically smaller in size than their factorisable counterparts. They can however grow to become significantly larger than the factorisable corrections when the jet transverse momenta become large, reaching $\mathcal{O}(40\%)$ level for $p_{t,j_2} \sim 160$ GeV, see figure 14. Once more, we can trace this back to the same mechanism described above:

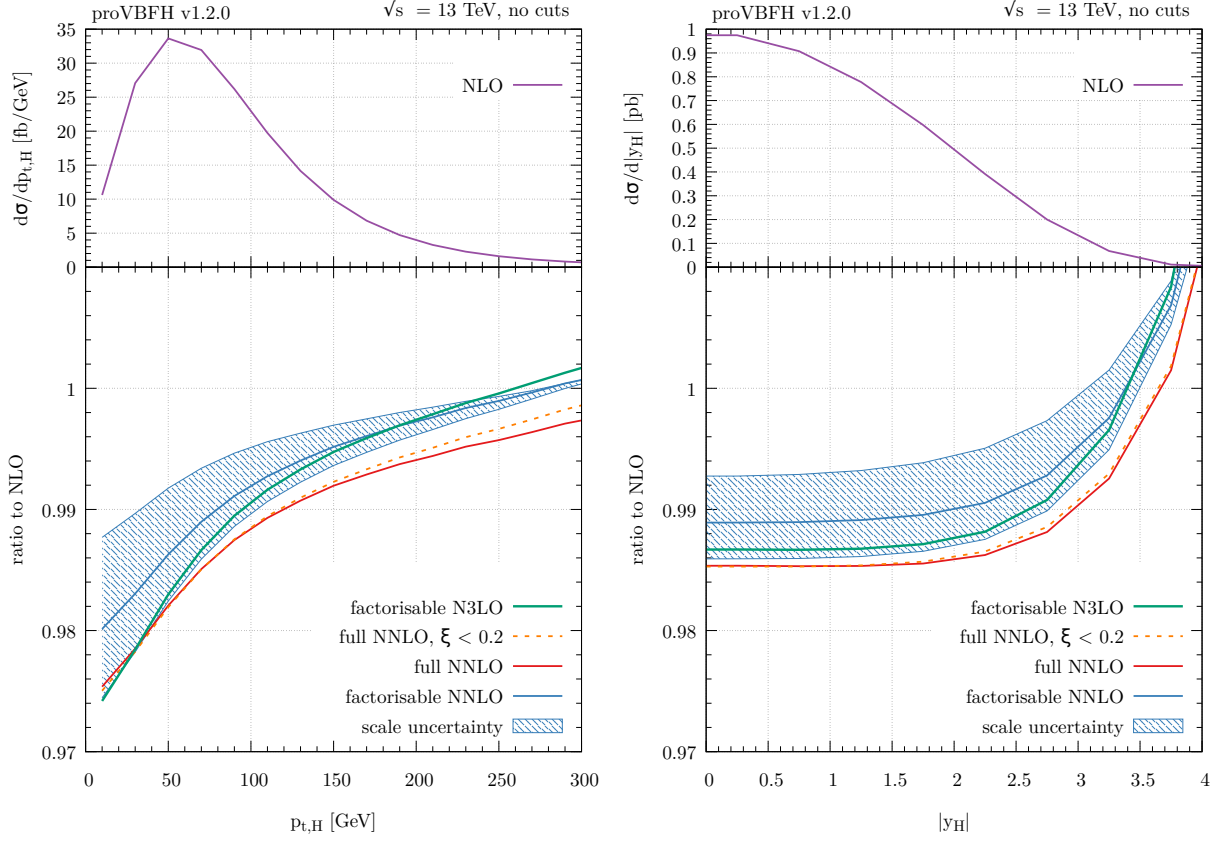


Fig. 12: Upper panel: NLO prediction for inclusive VBF production for the transverse momentum and rapidity of the Higgs boson. Lower panel: Ratio of the factorisable NNLO prediction to NLO (blue) and of the full NNLO prediction to NLO (red). The blue bands represent the scale uncertainty of the NNLO factorisable prediction. The orange dashed curve shows the full NNLO prediction after applying a cut $\xi < 0.2$ on the non-factorisable component. The factorisable N³LO prediction is shown in green.

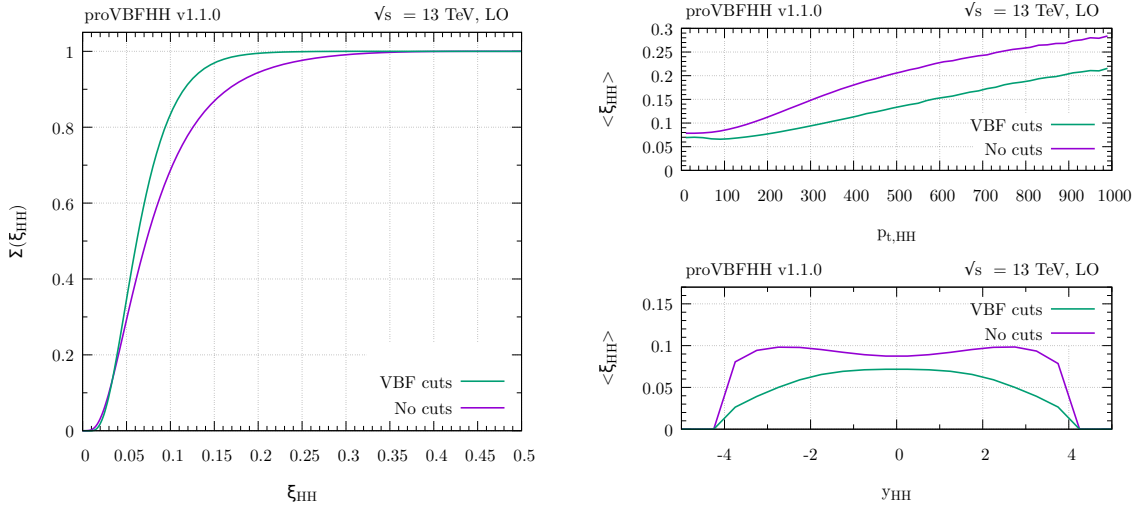


Fig. 13: Left: the normalised integrated cross section as a function of ξ fully inclusively (purple) and under the VBF cuts of sec. 3.1 (green) for di-Higgs production through VBF. Right: the average of ξ_{HH} as a function of y_{HH} and $p_{t,HH}$.

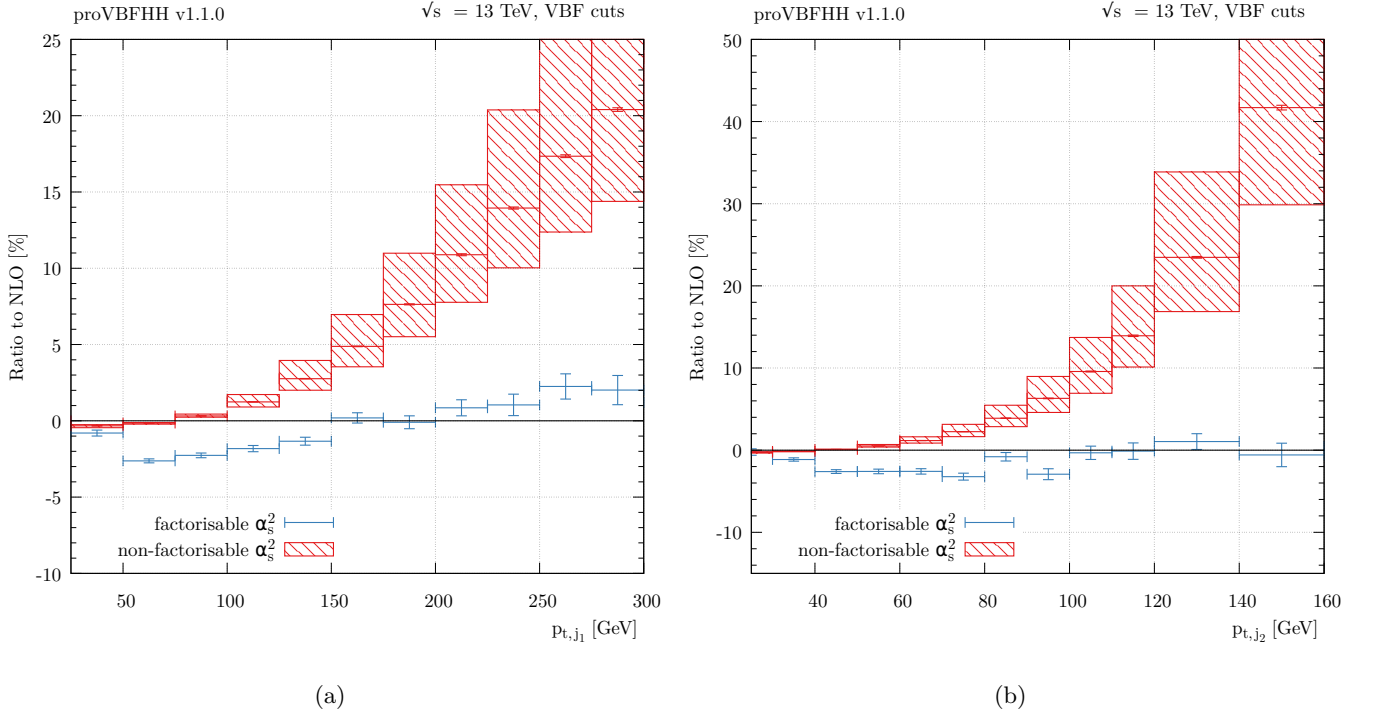


Fig. 14: Kinematic distributions for Higgs pair production through VBF under the cuts of sec. 3.1. (a) transverse momentum of the hardest jet (b) transverse momentum of the second hardest jet. In red we show the non-factorisable α_s^2 correction and in blue we show the factorisable one. Both are normalised to the NLO cross section.

the corrections to the individual Born contributions are not very large in this region, but the cancellation pattern between them is modified by QCD radiation, leading to very large corrections. We also note here that a similar growth of the NNLO non-factorisable corrections in the jet p_t distributions can be observed also in single Higgs production, see figure 10. Nevertheless, due to the lack of interference to enhance the corrections, these remain much more moderate than for double Higgs below $p_{t,j2} \sim 160$ GeV. We should also stress here that, as the jet transverse momenta grow, the eikonal approximation becomes less reliable and hence one should use the results in this region with caution.

In figure 15 we show the transverse momentum distribution of the Higgs with larger transverse momentum and of the di-Higgs system. Similar to the jet transverse momenta, we see an increase of the non-factorisable corrections when the Higgs bosons become hard. However, the corrections remain moderate, and tend to be of the same order of magnitude as the factorisable corrections.

Finally, in figure 16 we show the dijet rapidity separation and invariant mass. The non-factorisable corrections tend again to be small to moderate in both observables, and of the same order as the factorisable corrections.

VBF	$\sigma^{(\text{NLO fact.})}$	$\delta\sigma^{(\text{fact.})}$	$\delta\sigma^{(\text{non-fact.})}$
Hjj	0.876	$-0.032^{+0.008}_{-0.008}$	$-0.0030^{+0.0006}_{-0.0009}$ [pb]
$HHjj$	0.607	$-0.012^{+0.003}_{-0.001}$	$+0.010^{+0.005}_{-0.003}$ [fb]

Table 2: Fiducial cross sections for single and double Higgs VBF production at NLO, along with the corresponding NNLO corrections. The quoted uncertainties correspond to scale dependence, while statistical errors at NNLO are about 0.5%. For details on the scale variation see sec 3.1.

5 Conclusions

In this paper we have studied the relative sizes of factorisable and non-factorisable QCD corrections to both single and double VBF Higgs production. A summary of the results is given in table 2, which shows the NLO fiducial cross section of single and di-Higgs production and the corresponding NNLO corrections. This study was made possible by recent advances in estimating the non-factorisable terms contributing to the NNLO cross section [12], which we extended to the di-Higgs process. We have presented the combined factorisable and non-factorisable NNLO corrections, as implemented in the public code `proVBFH` v1.2.0 for single Higgs VBF production. We find that for typical selection cuts the non-factorisable NNLO corrections are small and mostly contained within the factorisable scale uncertainty bands. For large jet and Higgs transverse momenta,

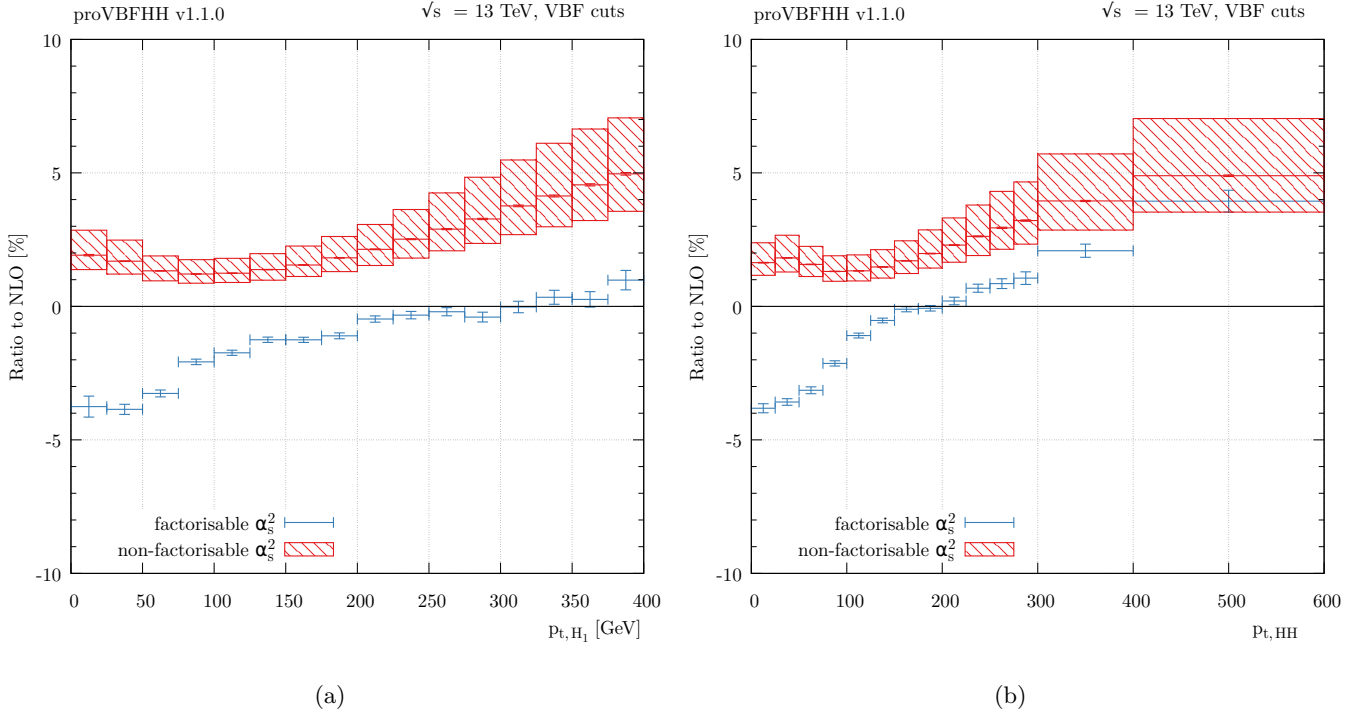


Fig. 15: Same as figure 14 for (a) transverse momentum of the hardest Higgs boson (b) transverse momentum of the di-Higgs system.

the non-factorisable corrections can become comparable to the factorisable ones. In this region, it is however not clear that the eikonal approximation used to estimate the corrections remains valid.

We also showed that the corrections computed in Ref. [12] can be used to provide an estimate for the non-factorisable corrections for the fully inclusive VBF phase space. In this case we find that the non-factorisable NNLO corrections are of the same order as the NNLO factorisable corrections, and moderately larger than the factorisable N^3 LO corrections. This is in contrast with the usual statement that non-factorisable corrections can be neglected at this order [5] for inclusive quantities. We stress that this estimate comes from an extrapolation of the eikonal approximation into a regime beyond where it is expected to remain valid, and should therefore only be taken as an estimation of the true size of non-factorisable NNLO corrections to fully inclusive VBF.

Finally, we have implemented the non-factorisable correction to the Higgs pair production process in VBF, which is available in proVBFHH v1.1.0. In di-Higgs production, we found that the non-factorisable corrections are sizable. This enhancement of the non-factorisable corrections comes from a delicate cancellation of the various Born diagrams, which is spoiled by the radiative corrections. Because the factorisable corrections to the di-Higgs process are smaller than in the single Higgs process, this leads to the non-factorisable corrections being of the same order of magnitude or even dominant compared to the NNLO factorisable

ones. For the fiducial volume studied here the two corrections have opposite sign and partially cancel each other.

Public versions of the codes used in this article are available online [40]. These results pave the way for precision measurements of the Higgs sector at the LHC and HL-LHC, as well as for further studies of non-factorisable effects and their interplay with the choice of jet radius.

Acknowledgments: We would like to thank Kirill Melnikov, Fabrizio Caola, and Thomas Gehrmann for many enlightening discussions. L.T. wishes to thank Ettore Remiddi and David Kosower for clarifying discussions on the reduction of loop integrals in two dimensions. We are also grateful to Kirill Melnikov, Gavin Salam, and Giulia Zanderighi for useful comments on the manuscript. F.D. is supported by the Science and Technology Facilities Council (STFC) under grant ST/P000770/1. A.K. is supported by the European Research Council (ERC) under the European Union’s Horizon 2020 research and innovation programme (grant agreement No. 788223, PanScales), and by Linacre College, Oxford. A.K. acknowledges support from the Swiss National Science Foundation (SNF) under grant number 200020-175595 while part of this work was carried out. L.T. is supported by the Royal Society through grant URF/R1/191125.

A Analytic results for one-loop integrals

In this appendix we report, for completeness, analytic results for the one-loop functions defined in eqs. (16,17) and in eqs. (19,21).

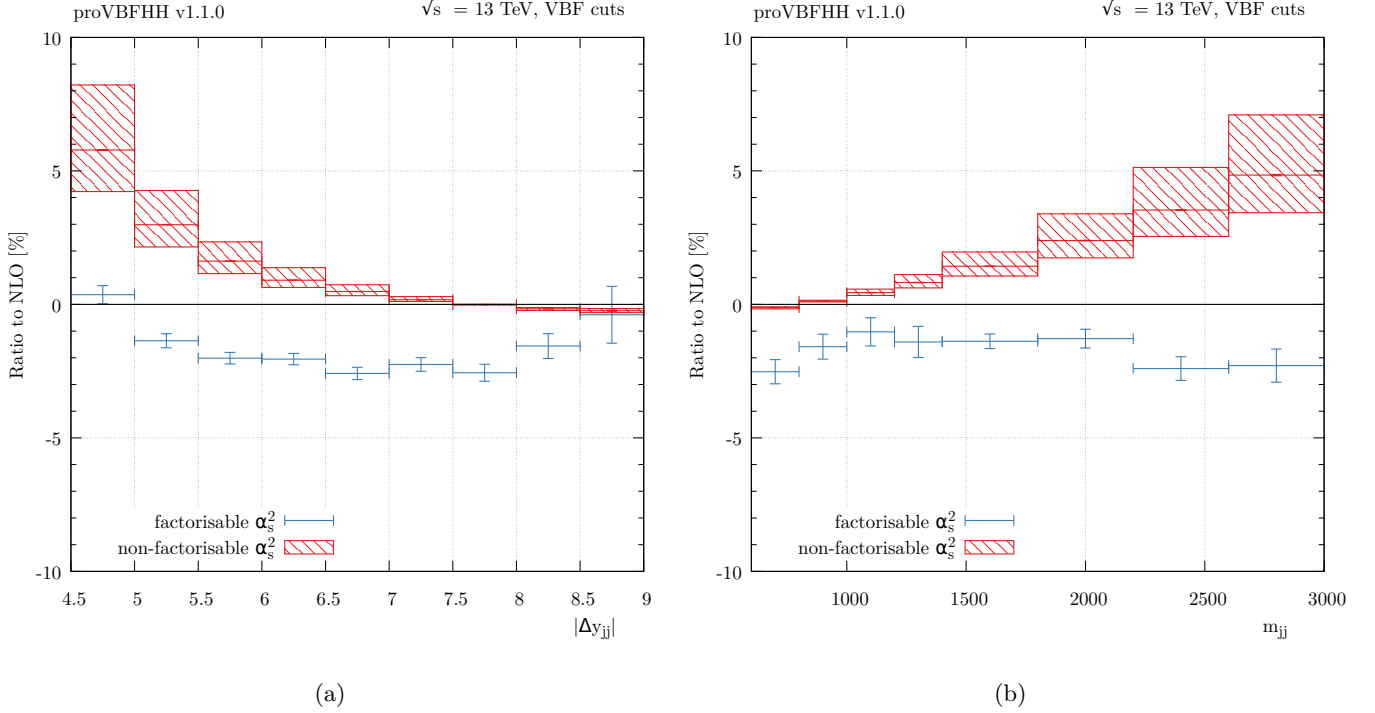


Fig. 16: Same as figure 14 for (a) dijet rapidity separation (b) dijet invariant mass.

We recall here that we are dealing with two-dimensional (euclidean) integrals. As it is well known, at one-loop any n -point function with $n \geq 3$ can be reduced to bubbles and tadpoles, such that the finite piece of every one-loop integral close to $d = 2$ dimensions can always be expressed in terms of logarithms only. We stress that, obviously, for this reduction to be true, one needs to work with explicitly two-dimensional kinematics. As in the main text, we parametrise the momenta q_1 , q_2 and q_3 as

$$\vec{q}_1 = (q_{1x}, 0), \quad \vec{q}_2 = (q_{2x}, q_{2y}), \quad \vec{q}_3 = (q_{3x}, q_{3y}) \quad (41)$$

such that the usual Mandelstam invariants are not independent and can be written as

$$s = (q_{1x} + q_{2x})^2 + q_{2y}^2, \quad t = (q_{1x} + q_{3x})^2 + q_{3y}^2, \quad (42)$$

$$u = (q_{2x} + q_{3x})^2 + (q_{2y} + q_{3y})^2, \quad (43)$$

$$q_1^2 = q_x^2, \quad q_2^2 = q_{2x}^2 + q_{2y}^2, \quad q_3^2 = q_{3x}^2 + q_{3y}^2, \quad (44)$$

$$q_4^2 = (q_x + q_{2x} + q_{3x})^2 + (q_{2y} + q_{3y})^2. \quad (45)$$

In what follows, we will use interchangeably either the Mandelstam invariants or their parametrisation above, depending on which of the two is more convenient.

In order to present the results below, we introduce a one-loop box family of finite, two-dimensional integrals

$$I_{n_1, n_2, n_3, n_4} = \frac{1}{\pi} \int d^2 \vec{k} \frac{1}{D_1^{n_1} D_2^{n_2} D_3^{n_3} D_4^{n_4}} \quad (46)$$

with $\sum_j n_j \geq 2$ and

$$D_1 = \vec{k}^2 + \lambda^2, \quad (47)$$

$$D_2 = (\vec{k} - \vec{q}_1)^2 + M_V^2, \quad (48)$$

$$D_3 = (\vec{k} + \vec{q}_2)^2 + M_V^2, \quad (49)$$

$$D_4 = (\vec{k} - \vec{q}_{13})^2 + M_V^2. \quad (50)$$

With this notation we see that

$$\chi_T^{(1)}(\vec{q}_1, \vec{q}_2) = I_{1,1,1,0}, \quad \chi_{B_1}^{(1)}(\vec{q}_1, \vec{q}_2, \vec{q}_3) = I_{1,1,1,1}.$$

It is very easy to reduce the box-integral $I_{1,1,1,1}$ to triangle integrals by noticing that, for strictly two-dimensional kinematics, the four propagators D_j are not linearly independent and one can write

$$1 = \frac{1}{\Delta_B} \left[(2q_{2y}q_{3x} - (q_{3y}(q_{1x} + 2q_{2x})) D_1 + q_{1x}q_{2y}(D_4 - D_2) + q_{1x}q_{3y}D_3 \right] \quad (51)$$

with

$$\Delta_B = M_V^2 q_{1x} q_{3y} + \lambda^2 (2q_{3x} q_{2y} - q_{1x} q_{3y} - 2q_{2x} q_{3y}) + q_{1x} (q_{2x}^2 q_{3y} + q_{3x}^2 q_{2y} + 2q_{1x} q_{3x} q_{2y} + q_{2y}^2 q_{3y} + q_{2y}^2 q_{3y}). \quad (52)$$

Using this equation in the numerator of $I_{1,1,1,1}$ one easily finds

$$I_{1,1,1,1} = \frac{1}{\Delta_B} \left[(2q_{2y}q_{3x} - (q_{3y}(q_{1x} + 2q_{2x})) I_{0,1,1,1} + q_{1x}q_{2y}(I_{1,1,1,0} - I_{1,0,1,1}) + q_{1x}q_{3y}I_{1,1,0,1}) \right], \quad (53)$$

which reduces the box to a combination of four triangles. We stress here that eq. (51) is actually a reduction at the *integrand level*. In other words, it only assumes two-dimensional kinematics but does not require any conditions on the dimensions of the loop momentum \vec{k} . Indeed, the relation can be used to reduce the box-integral $I_{1,1,1,1}$ to triangles exactly even if the loop integration were to be performed in d dimensions.

As it is well known, in $d = 2$ triangles are also not independent and can in turn be reduced to bubbles. Contrary to eq. (53), the reduction of triangles to bubbles is only true at the *integral level*, i.e. it assumes that also the loop momentum is two-dimensional. To proceed, let us first notice that since $I_{1,0,1,1}$ and $I_{1,1,0,1}$ can be obtained from $I_{1,1,1,0}$ simply by permuting the external invariants, we only need to study $I_{1,1,1,0}$ and $I_{0,1,1,1}$.

We start with $I_{1,1,1,0}$, whose integrand depends on the three momenta $\vec{q}_1, \vec{q}_2, \vec{k}$. If the loop momentum is also two-dimensional, then it is immediate to see that the Gram determinant of the three vectors $G(\vec{k}, \vec{q}_1, \vec{q}_2)$ must be zero. We can then write down the identity

$$\int d^2\vec{k} \frac{G(\vec{k}, \vec{q}_1, \vec{q}_2)}{D_1^{n_1} D_2^{n_2} D_3^{n_3}} = 0 \quad (54)$$

which is identically true for every $n_1, n_2, n_3 \in \mathbb{N}$ such that the integral converges. After reducing all integrals to triangles and bubbles and using $\lambda = 0$ for simplicity,¹ can be inverted to give

$$I_{1,1,1,0} = \frac{1}{\Delta_{T,1}} \left[s(q_1^2 + q_2^2 - s - 2M_V^2) I_{0,1,1,0} + (q_2^2(M_V^2 + q_1^2 + s) - q_2^4 - M_V^2(q_1^2 - s)) I_{1,0,1,0} + (M_V^2(q_1^2 - q_2^2 + s) - q_1^2(q_1^2 - q_2^2 - s)) I_{1,1,0,0} \right] \quad (55)$$

where

$$\Delta_{T,1} = 2 \left[M_V^4 s + M_V^2(q_1^2(2q_2^2 + s) + q_2^2(s - q_2^2) - q_1^4) + q_1^2 q_2^2 s \right]. \quad (56)$$

Repeating the very same steps for $I_{0,1,1,1}$, using instead the Gram determinant $G(\vec{k}, \vec{q}_3, \vec{q}_4)$ one finds

$$I_{0,1,1,1} = \frac{1}{\Delta_{T,2}} \left[q_3^2(s - q_3^2 + q_4^2) I_{0,1,0,1} + q_4^2(s + q_3^2 - q_4^2) I_{0,0,1,1} + s(q_3^2 + q_4^2 - s) I_{0,1,1,0} \right] \quad (57)$$

¹ We are interested in the value of the integral in the limit $\lambda \rightarrow 0$, where we know that it can only develop a logarithmic singularity.

with

$$\Delta_{T,2} = 2 \left[M_V^2 \left((s - q_4^2)^2 + q_3^4 \right) + q_3^2 q_4^2 s - 2q_3^2(q_4^2 + s) \right]. \quad (58)$$

We stress once more that in $d = 2$ the 6 Mandelstam invariants $s, t, q_1^2, q_2^2, q_3^2, q_4^2$ are not independent and therefore the relations above are not unique.

Finally, we are left with the computation of the one-loop bubbles, which is entirely straightforward. We report here the results for completeness

$$I_{1,1,0,0} = \frac{1}{\Delta_1} \left[2 \ln \left(\frac{\Delta_1}{M_V^2} \right) - \ln \left(\frac{\lambda^2}{M_V^2} \right) \right] \quad (59)$$

$$I_{0,1,1,0} = \frac{2}{\sqrt{s(s + 4M_V^2)}} \ln \left(\frac{\sqrt{s + 4M_V^2} + \sqrt{s}}{\sqrt{s + 4M_V^2} - \sqrt{s}} \right) \quad (60)$$

$$I_{1,0,1,0} = I_{1,1,0,0} \Big|_{\Delta_1 \rightarrow \Delta_2}, \quad I_{1,0,0,1} = I_{1,1,0,0} \Big|_{\Delta_1 \rightarrow \Delta_t} \quad (61)$$

$$I_{0,1,0,1} = I_{0,1,1,0} \Big|_{s \rightarrow \vec{q}_3^2}, \quad I_{0,0,1,1} = I_{0,1,1,0} \Big|_{s \rightarrow \vec{q}_4^2} \quad (62)$$

where we recall the definitions

$$\Delta_1 = \vec{q}_1^2 + M_V^2, \quad \Delta_2 = \vec{q}_2^2 + M_V^2, \quad \Delta_t = t + M_V^2. \quad (63)$$

References

1. **ATLAS Collaboration** Collaboration, G. Aad *et al.*, *Observation of a new particle in the search for the Standard Model Higgs boson with the ATLAS detector at the LHC*. Phys.Lett. **B716** (2012) 1–29, [arXiv:1207.7214 \[hep-ex\]](#).
2. **CMS Collaboration**, S. Chatrchyan *et al.*, *Observation of a New Boson at a Mass of 125 GeV with the CMS Experiment at the LHC*. Phys. Lett. **B716** (2012) 30–61, [arXiv:1207.7235 \[hep-ex\]](#).
3. J. Alison *et al.*, “Higgs Boson Pair Production at Colliders: Status and Perspectives,” in *Double Higgs Production at Colliders*, B. Di Micco, M. Gouzevitch, J. Mazitelli, and C. Vernieri, eds. 9, 2019. [arXiv:1910.00012 \[hep-ph\]](#).
4. T. Figy, C. Oleari, and D. Zeppenfeld, *Next-to-leading order jet distributions for Higgs boson production via weak boson fusion*. Phys. Rev. **D68** (2003) 073005, [arXiv:hep-ph/0306109 \[hep-ph\]](#).
5. P. Bolzoni, F. Maltoni, S.-O. Moch, and M. Zaro, *Higgs production via vector-boson fusion at NNLO in QCD*. Phys. Rev. Lett. **105** (2010) 011801, [arXiv:1003.4451 \[hep-ph\]](#).
6. B. Jäger, F. Schissler, and D. Zeppenfeld, *Parton-shower effects on Higgs boson production via vector-boson fusion in association with three jets*. JHEP **07** (2014) 125, [arXiv:1405.6950 \[hep-ph\]](#).
7. M. Cacciari, F. A. Dreyer, A. Karlberg, G. P. Salam, and G. Zanderighi, *Fully Differential Vector-Boson-Fusion Higgs Production at Next-to-Next-to-Leading Order*. Phys. Rev. Lett. **115** (2015) no. 8, 082002, [arXiv:1506.02660 \[hep-ph\]](#).

8. J. Cruz-Martinez, T. Gehrmann, E. W. N. Glover, and A. Huss, *Second-order QCD effects in Higgs boson production through vector boson fusion*. Phys. Lett. **B781** (2018) 672–677, [arXiv:1802.02445 \[hep-ph\]](#).
9. F. A. Dreyer and A. Karlberg, *Vector-Boson Fusion Higgs Production at Three Loops in QCD*. Phys. Rev. Lett. **117** (2016) no. 7, 072001, [arXiv:1606.00840 \[hep-ph\]](#).
10. F. Campanario, T. M. Figy, S. Plätzer, M. Rauch, P. Schichtel, and M. Sjödal, *Stress testing the vector-boson-fusion approximation in multijet final states*. Phys. Rev. D **98** (2018) no. 3, 033003, [arXiv:1802.09955 \[hep-ph\]](#).
11. T. Han, G. Valencia, and S. Willenbrock, *Structure function approach to vector boson scattering in $p p$ collisions*. Phys. Rev. Lett. **69** (1992) 3274–3277, [arXiv:hep-ph/9206246 \[hep-ph\]](#).
12. T. Liu, K. Melnikov, and A. A. Penin, *Nonfactorizable QCD Effects in Higgs Boson Production via Vector Boson Fusion*. [arXiv:1906.10899 \[hep-ph\]](#).
13. M. Ciccolini, A. Denner, and S. Dittmaier, *Electroweak and QCD corrections to Higgs production via vector-boson fusion at the LHC*. Phys. Rev. **D77** (2008) 013002, [arXiv:0710.4749 \[hep-ph\]](#).
14. R. V. Harlander, J. Vollinga, and M. M. Weber, *Gluon-Induced Weak Boson Fusion*. Phys. Rev. **D77** (2008) 053010, [arXiv:0801.3355 \[hep-ph\]](#).
15. J. R. Andersen, T. Binoth, G. Heinrich, and J. M. Smillie, *Loop induced interference effects in Higgs Boson plus two jet production at the LHC*. JHEP **02** (2008) 057, [arXiv:0709.3513 \[hep-ph\]](#).
16. A. Vogt, S. Moch, and J. A. M. Vermaseren, *The Three-loop splitting functions in QCD: The Singlet case*. Nucl. Phys. **B691** (2004) 129–181, [arXiv:hep-ph/0404111 \[hep-ph\]](#).
17. S. Moch, J. A. M. Vermaseren, and A. Vogt, *The Longitudinal structure function at the third order*. Phys. Lett. **B606** (2005) 123–129, [arXiv:hep-ph/0411112 \[hep-ph\]](#).
18. J. A. M. Vermaseren, A. Vogt, and S. Moch, *The Third-order QCD corrections to deep-inelastic scattering by photon exchange*. Nucl. Phys. **B724** (2005) 3–182, [arXiv:hep-ph/0504242 \[hep-ph\]](#).
19. S. Moch, M. Rogal, and A. Vogt, *Differences between charged-current coefficient functions*. Nucl. Phys. **B790** (2008) 317–335, [arXiv:0708.3731 \[hep-ph\]](#).
20. S. Buehler and C. Duhr, *CHAPLIN - Complex Harmonic Polylogarithms in Fortran*. Comput. Phys. Commun. **185** (2014) 2703–2713, [arXiv:1106.5739 \[hep-ph\]](#).
21. A. Dobrovolskaya and V. Novikov, *On heavy Higgs boson production*. Z. Phys. **C52** (1991) 427–436.
22. H. Cheng and T. T. Wu, *High-energy collision processes in quantum electrodynamics. iii*. Phys. Rev. **182** (1969) 1873–1898.
23. S.-J. Chang and S.-K. Ma, *Multiphoton exchange amplitudes at infinite energy*. Phys. Rev. **188** (1969) 2385–2404.
24. H. Cheng and T. T. Wu, *Impact factor and exponentiation in high-energy scattering processes*. Phys. Rev. **186** (1969) 1611–1618.
25. L. N. Lipatov, *Reggeization of the Vector Meson and the Vacuum Singularity in Nonabelian Gauge Theories*. Sov. J. Nucl. Phys. **23** (1976) 338–345. [*Yad. Fiz.* 23,642(1976)].
26. F. Campanario, T. M. Figy, S. Plätzer, and M. Sjödal, *Electroweak Higgs Boson Plus Three Jet Production at Next-to-Leading-Order QCD*. Phys. Rev. Lett. **111** (2013) no. 21, 211802, [arXiv:1308.2932 \[hep-ph\]](#).
27. NNPDF Collaboration, R. D. Ball *et al.*, *Parton distributions for the LHC Run II*. JHEP **04** (2015) 040, [arXiv:1410.8849 \[hep-ph\]](#).
28. A. Buckley, J. Ferrando, S. Lloyd, K. Nordström, B. Page, M. Rüfenacht, M. Schönherr, and G. Watt, *LHAPDF6: parton density access in the LHC precision era*. Eur. Phys. J. **C75** (2015) 132, [arXiv:1412.7420 \[hep-ph\]](#).
29. ATLAS, CMS Collaboration, G. Aad *et al.*, *Combined Measurement of the Higgs Boson Mass in pp Collisions at $\sqrt{s} = 7$ and 8 TeV with the ATLAS and CMS Experiments*. Phys. Rev. Lett. **114** (2015) 191803, [arXiv:1503.07589 \[hep-ex\]](#).
30. M. Cacciari, G. P. Salam, and G. Soyez, *The Anti- $k(t)$ jet clustering algorithm*. JHEP **0804** (2008) 063, [arXiv:0802.1189 \[hep-ph\]](#).
31. M. Cacciari, G. P. Salam, and G. Soyez, *FastJet User Manual*. Eur. Phys. J. **C72** (2012) 1896, [arXiv:1111.6097 \[hep-ph\]](#).
32. G. P. Salam and J. Rojo, *A Higher Order Perturbative Parton Evolution Toolkit (HOPPET)*. Comput. Phys. Commun. **180** (2009) 120–156, [arXiv:0804.3755 \[hep-ph\]](#).
33. S. Alioli, P. Nason, C. Oleari, and E. Re, *A general framework for implementing NLO calculations in shower Monte Carlo programs: the POWHEG BOX*. JHEP **1006** (2010) 043, [arXiv:1002.2581 \[hep-ph\]](#).
34. P. Nason and C. Oleari, *NLO Higgs boson production via vector-boson fusion matched with shower in POWHEG*. JHEP **02** (2010) 037, [arXiv:0911.5299 \[hep-ph\]](#).
35. CMS Collaboration, V. Khachatryan *et al.*, *Search for the standard model Higgs boson produced through vector boson fusion and decaying to $b\bar{b}$* . Phys. Rev. **D92** (2015) no. 3, 032008, [arXiv:1506.01010 \[hep-ex\]](#).
36. ATLAS Collaboration, M. Aaboud *et al.*, *Search for Higgs bosons produced via vector-boson fusion and decaying into bottom quark pairs in $\sqrt{s} = 13$ TeV pp collisions with the ATLAS detector*. Phys. Rev. **D98** (2018) no. 5, 052003, [arXiv:1807.08639 \[hep-ex\]](#).
37. M. Rauch and D. Zeppenfeld, *Jet clustering dependence of Higgs boson production in vector-boson fusion*. Phys. Rev. **D95** (2017) no. 11, 114015, [arXiv:1703.05676 \[hep-ph\]](#).

- 38. F. A. Dreyer and A. Karlberg, *Fully differential Vector-Boson Fusion Higgs Pair Production at Next-to-Next-to-Leading Order*. Phys. Rev. **D99** (2019) no. 7, 074028, [arXiv:1811.07918 \[hep-ph\]](#).
- 39. F. A. Dreyer and A. Karlberg, *Vector-Boson Fusion Higgs Pair Production at N^3LO* . Phys. Rev. **D98** (2018) no. 11, 114016, [arXiv:1811.07906 \[hep-ph\]](#).
- 40. proVBFH. <http://provbhf.hepforge.org/>.